Investigation of the effect of modular construction details on the lateral behaviour of cold-formed steel framed shear walls

Smail Kechidi [a,b,*], Ornella Iuorio [a]

[a] School of Civil Engineering, University of Leeds, Leeds, United Kingdom
[b] ilke Homes Ltd., Knaresborough, United Kingdom

ARTICLE INFO

ABSTRACT

This paper investigates the effect of modular construction details on laterally-loaded cold-formed steel (CFS) framed shear walls sheathed with wood- and cement-based panels by means of finite-element (FE) analyses. Shell FE-based models have been developed in ABAQUS with the aim of accurately capturing the behaviour, strength and stiffness as well as the corresponding failure modes of CFS framed shear walls subjected to monotonic lateral load (*i.e.*, wind). User-defined element subroutines were adopted for precise modelling of sheathing-to-CFS screws shear behaviour. The proposed modelling protocol is validated using experimental test results, where an acceptable concordance (4% difference) has been achieved. Subsequently, the effect of modular construction details, which go beyond the scope of the current lateral design provisions (AISI S400), on the lateral behaviour of CFS framed shear walls is assessed. In particular, this paper investigates the impact of: (i) floor and ceiling ledger beams on the interior face of the shear wall, (ii) sheathing boards having different sizes from the overall shear wall and thus the presence of both vertical and horizontal seams, (iii) cement particle boards at the bottom stripe of the shear wall and (iv) different screw spacing in the top and bottom stripes from the middle part of the shear wall. The key parameters, which have most affected the lateral behaviour, were identified, and based on that, rules have been established for optimizing the screws pattern and sheathings layout efficacy in the above-described lateral load resisting system. The obtained results shed light on the capability of the developed modelling protocol to be used as a virtual test bench, particularly in offsite mass production and manufacture (DfMA), for the development of a new CFS framed wall system for lateral stability of lightweight modular houses.

1. Introduction

In recent years, structural- and cost-efficiency, durability as well as sustainability [1] have ramped-up the use of cold-formed steel (CFS) profiles in many countries as both structural and non-structural elements [2]. Shear walls made of CFS members (studs, tracks and blockings) and sheathed with wood or cement particle (CP) panels are one of the lateral load resisting systems (LLRSs) adopted in lightweight steel construction [3]. The main codes that currently define methodologies for the design of CFS structures are AISI S400 (2015) [4] and AS/NZS 4600 (2018) [5]. However, in the current market, CFS modular buildings can include construction details that could influence their lateral behaviour, and are not covered by the current lateral design provisions and guidelines for CFS structures [4]. Furthermore, the complex analyses and design procedures related to the significant number of thin components, which are locally unstable and show several failure

mechanisms, require an advanced lateral behaviour investigation [6]. For the past two decades, full-scale testing has been largely adopted to investigate the behaviour of CFS framed shear walls under lateral loads [7–11], posing the basis for design and code development.

Virtual testing (*i.e.*, numerical simulation) has also been largely adopted for advancing understating of CFS structural capacity and predict their behaviour at varying of loading conditions and structural components, to the point that now it can be deemed of primary importance for the purpose of optimizing the structural performance of the CFS framed buildings, in particular, at the early stages of the product development process.

Over the last decade, several endeavours have been devoted to the numerical simulation of CFS framed shear walls subjected to monotonic and cyclic (quasi-static and dynamic) lateral load. Stewart model (1987) [12] was deemed suitable for the simulation of the experimental tests carried out by Nisreen Balh (2010) [13] on CFS framed shear walls,
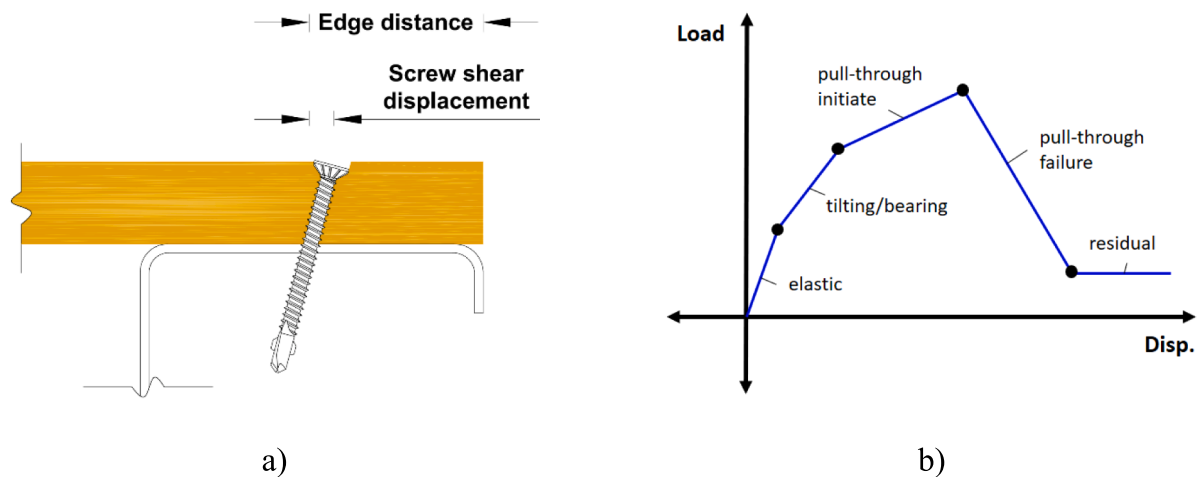

Fig. 1. Sheathing-to-CFS screw: a) interaction and b) typical shear behaviour.

however, the strength deterioration observed in the test results was not considered. Martínez and Xu (2010) [14] proposed a simplified, yet accurate, approach for modelling a CFS framed shear wall using a 16-node shell element with equivalent geometric and material properties derived from the actual properties of a CFS framed shear wall. Liu P. et al (2012) [15] adopted Pinching4 model [16] developed by Lowes and Altoontash (2003) [17] in order to characterize the cyclic behaviour of CFS wood-sheathed shear walls; this model was calibrated based on experimental test results and reproduced the hysteretic behaviour with an acceptable accuracy (below 10 % difference). Based on the same model, 2- and 3-dimensional models were established by Leng J. et al. (2017) [18] for nonlinear dynamic response history analyses of full CFS systems (2-storey buildings). Shamim and Rogers (2013) [19] simulated the nonlinear response history of two-storey CFS framed shear walls under seismic load using Pinching4 model that was calibrated based on results of dynamic tests carried out by the same authors. Vigh et al. (2014) [20] developed and calibrated a simplified strut model with the adoption of the Ibarra-Medina-Krawinkler constitutive model [21] to represent the deteriorating hysteretic loops of CFS corrugated steel-sheathed shear walls. Buonopane et al. (2015) [22] developed a computationally efficient screw-based modelling protocol in OpenSees software for CFS OSB-sheathed shear walls. Two hysteretic models that take into account strength and stiffness deterioration as well as pinching, have been developed and implemented in the official OpenSees release (version 2.4.5 and above) by Kechidi and Bourahla (2016) [23] to simulate CFS wood- and steel-sheathed shear walls behaviour under monotonic and cyclic lateral load. It is worth noting that all the above-described numerical simulations adopted beam-column elements to model the CFS frame members. Consequently, local and distortional buckling or their combination were not captured. David Padilla-Llano (2015) [24] proposed a numerical framework for CFS framed shear walls that captures the nonlinear cyclic behaviour of critical components including frame members (chord studs) as well as screws. More advanced modelling techniques have been undertaken by Hung Huy Ngo (2014) [25] through the adoption of SpringA element in ABAQUS to simulate the shear behaviour of the screws connecting OSB sheathing to CFS frame members. Deverni et al. (2021) [26–27] replicated the same efforts with a simplistic approach of modelling the shear behaviour of the sheathing-to-CFS screws using CONN3D2 element in ABAQUS assuming a constant angle between the screw deformation and the global horizontal axis throughout all levels of lateral demand on the shear wall. Moreover, with no un- and re-loading paths defined, SpringA and CONN3D2 elements can merely be adopted in the simulation of the lateral behaviour of CFS shear walls under monotonic load. The Bouc–Wen–Baber–Noori (BWBN) (1993) [28] model was used by Nithyadharan and Kalyanaraman (2013) [29] to capture the

deteriorating behaviour, in terms of strength and stiffness deterioration with severe pinching, that has been observed in the screw fasteners between the sheathing and CFS frame members under cyclic load. Subsequently, the BWBN constitutive model along with a variably oriented spring pair element have been implemented in ABAQUS as a user-element (UEL) to replicate the cyclic behaviour of the screws under shear demand [30]. In all the above-described modelling efforts, the aim was to replicate the results of tests on conventional CFS framed shear walls rather than optimizing the structural performance of CFS framed shear walls with constructional details that are not covered by the current lateral design provisions and guidelines.

The innovation in the study presented in this paper is to uncover the effect of modular construction details on the behaviour of laterally-loaded CFS framed shear walls and to optimize the screws pattern and sheathings layout efficacy in this LLRS. Therefore in this paper, first experimental tests on sheathing-to-CFS screws (Section 2) and tensile tests on CFS frame members (Section 3) are presented to characterize the basic components of the shear walls under investigation. An advanced modelling protocol is proposed in Section 4, which uses radial springs with experimentally-derived backbone curves implemented in UELs, to model the shear behaviour of sheathing-to-CFS screws, while accounting for the deformation of the shear wall frame members. The proposed modelling protocol is validated using results coming from experimental tests carried out by the authors [31], where a good agreement has been achieved. Subsequently, the effect of additional details that are commonly adopted in CFS modular construction and go beyond the scope of the current lateral design provisions is assessed (Sections 5, 6 and 7). The main details include: *(i)* presence of floor and ceiling ledger beams on the interior face of the shear wall, *(ii)* sheathing boards having different sizes from the overall shear wall and thus the presence of both vertical and horizontal seams, *(iii)* use of cement particle (CP) boards at the bottom stripe of the shear wall and *(iv)* different screw spacing in the top and bottom stripes from the middle part of the shear wall. Lastly, rules have been established for optimizing the screws pattern and sheathings layout efficacy in the above-described LLRS.

2. Sheathing-to-CFS screw shear tests

In CFS framed shear walls all framing elements are considered pin jointed (no moment is allowed to develop at the joint). The stability of the wall system is therefore provided by the shear strength and stiffness that originate from the screw shear displacement demand. Fig. 1 shows a typical behaviour of sheathing-to-CFS screw characterized by tilting and bearing against the sheathing board of the screw followed by pull-through which continues until failure occurs. For screws with small edge distance, it is possible that the second and/or third branch is cut off
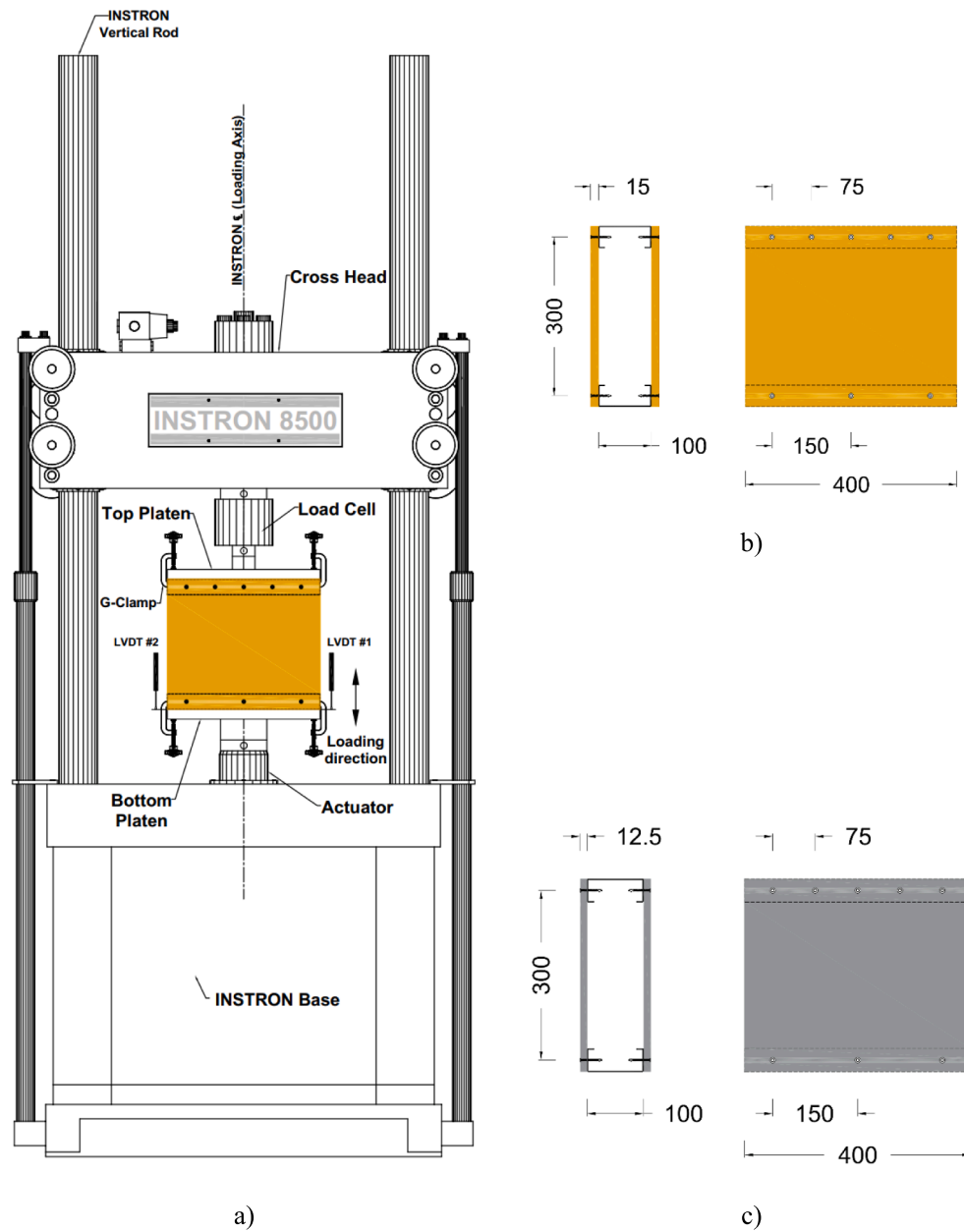
Fig. 2. Sheathing-to-CFS screw shear test setup, a) front view of specimen in rig, b) OSB- and c) CP-sheathed specimen dimensions (in mm) and details.
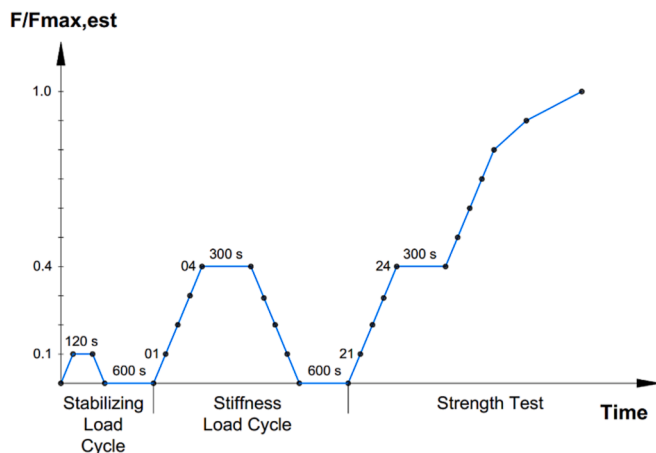

Fig. 3. BS EN 594: 1996 loading protocol [33].

by tear out in the sheathing. Therefore, it is deemed necessary to characterize the shear behaviour of the sheathing-to-CFS screws. Twelve tests on screws connecting oriented strand boards (OSB) and CP boards to CFS profiles have been carried out. The experiments investigate the sheathing type and thickness as well as the distance between the screw longitudinal axis and the edge of the sheathing (*i.e.*, the edge distance).

Table 1

Test matrix for characterizing the shear behaviour of OSB/CP-to-CFS screws.

| Steel thickness (mm) | Loading[a] | Edge distance (mm) | | | |
| | | 20.50 | | 10.25 | |
		OSB	CP	OSB	CP
1.6	Monotonic	3[b]	3[b]	3[b]	3[b]

Note: OSB = Oriented Strand Board (15 mm) and CP = Cement Particle (12.5 mm).

[a] Loading protocol is in accordance with the BS EN 594 (1996),
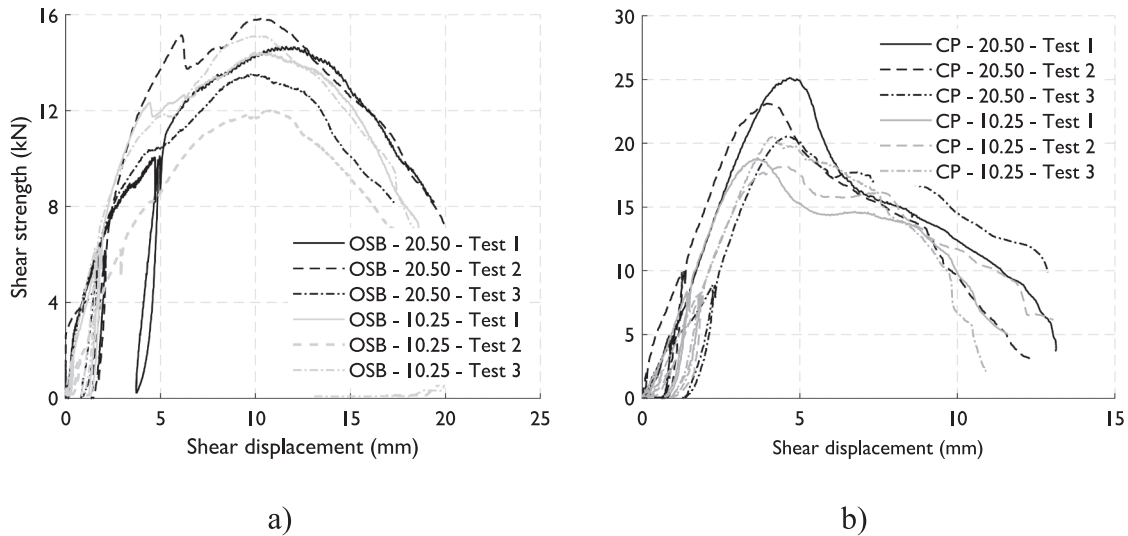[b] Indicates number of specimens per specimen variant.

Fig. 4. Load vs displacement curves for: a) OSB- and b) CP-sheathed specimens.

Table 2
Key sheathing-to-CFS screw shear test results.

Sheathing	Edge distance (mm)	Peak shear strength (kN)	Stiffness (kN/mm)	Disp. at peak shear strength (mm)	80 % peak shear strength (kN)	Disp. at 80 % post peak shear strength (mm)	Energy[a] (kN.mm)	Failure mode[b]
OSB	20.50	14.67	3.73	11.62	11.68	16.30	220.50	T + PT
		15.85	3.02	10.26	12.63	14.93	232.14	
		13.53	3.30	9.76	10.79	14.27	180.48	
CP		25.13	5.84	4.68	19.96	5.80	184.54	T + PT
		23.11	7.37	3.95	18.44	5.51	169.02	
		20.53	3.67	4.67	16.38	9.12	178.81	T + PT + E
OSB	10.25	14.42	3.09	9.99	11.48	15.64	219.67	T + PT
		12.03	2.24	10.93	9.63	14.46	174.51	
		15.11	4.05	10.40	12.07	14.67	219.84	
CP		18.76	5.28	3.70	14.95	5.17	141.78	T + E
		18.16	4.28	4.63	14.52	8.25	157.34	T + PT
		20.59	4.37	4.18	16.36	7.28	139.34	T + PT + E

[a] The strain energy is calculated as the area comprised between the load–displacement curve and the x-axis;
[b] T = tilting, PT = pull through and E = edge distance failure.

2.1. Test setup

Fig. 2 shows OSB- and CP-sheathed specimens and the testing rig that has been adopted to apply monotonic concentric compression load during this test campaign, so that the sheathing-to-CFS screws would be subjected to shear load. Indeed, although forces in the sheathing-to-CFS screws are parallel to the flanges of the frame members and at an angle of ~ 65 degree around the sheathing corners of CFS framed shear walls,
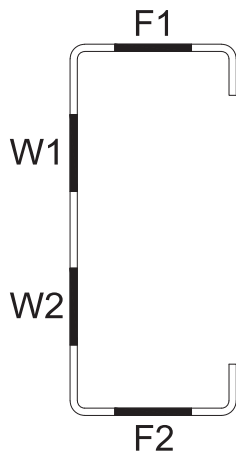
which is confirmed by the results presented in Section 6, the design of specimens was performed so that the direction of shear forces would be perpendicular to the specimens flanges assuming that the direction of force has no effect on the shear behaviour of the assembly as long as no tear out of the sheathing edge happens [32].

One lipped channel C100-41.3–1.6 was adopted to build the specimens shown in Fig. 2. The C100-41.3–1.6 has the following out-to-out nominal dimensions: a web depth of 100 mm, a flange width of 41.3 mm, a lip length of 11 mm and a thickness of 1.6 mm. This C-section is the same section type utilized in tests on the shear walls described in Section 4.1. OSB and CP sheathing of 400 × 341 mm (width × length) having, respectively, 15 and 12.5 mm thickness were attached on both sides of the studs and in contact with the flanges as shown in Fig. 2b and 2c.

As shown in Fig. 2a, the specimens are supported and loaded via, respectively, the top and bottom platens. The shear displacement is measured as the relative movement between the flanges of the C-section and the OSB/CP sheathing boards. Two LVDTs were placed on the web inner face of the C-section in order to measure the relative displacement between the bottom stud and sheathing boards. Measurements of load are made through the rig load cell (Fig. 2a).

Each specimen was subjected to the BS EN 594: 1996 [33] loading protocol. The BS EN 594 basic loading history, shown in Fig. 3, includes 3 cycles with specified load levels. All tests were displacement-controlled quasi-static, with the loading rate not exceeding 4.00 mm/min.
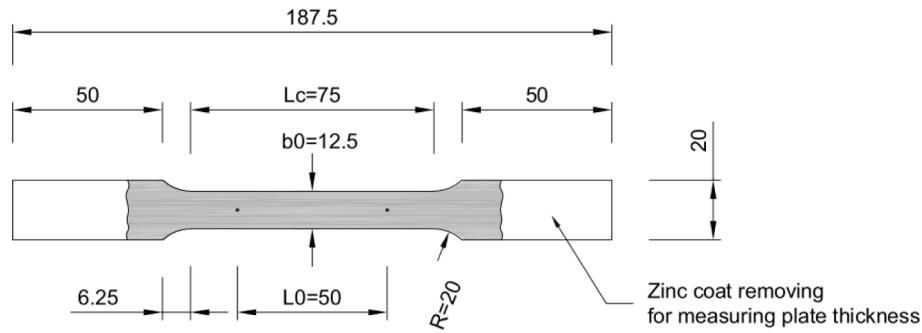

Fig. 5. Location of coupons taken from lipped channel cross-section.
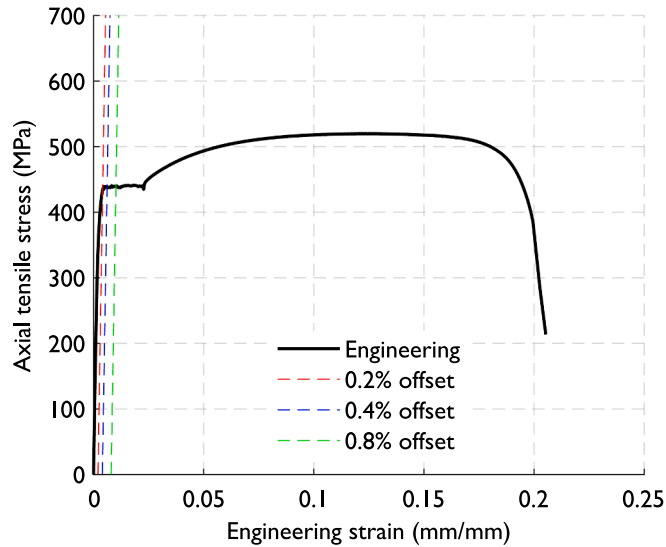
Fig. 6. Tensile coupon dimensions in mm.

Fig. 7. Stress vs strain of C100-41.3–1.6-F1 coupon.

2.2. Test specimens

Specimens were configured to represent typical sheathing-to-frame screws used in CFS framed shear wall assemblies that were subsequently tested by the authors (see Section 4). For this purpose, the tests investigated the main parameters that can most influence the lateral resistance of typical CFS framed shear walls and need to be defined before carrying out full-scale experimental tests. Therefore, the following parameters were studied: a) sheathing type and thickness and b) the edge distance.

Testing were conducted with self-drilling screws in the field of the OSB and CP as shown in Fig. 2b and 2c. The edge distance can significantly influence the ultimate shear strength and stiffness of the assembly [34], therefore, the screws are placed at 20.5 and 10.25 mm from the edge of the sheathing boards and spaced longitudinally at 150 mm (Fig. 2b and c).

The test parameters are summarized in the test matrix of Table 1. A minimum of three replicates of each test were performed.

2.3. Test results

Strength-displacement curves under monotonic load are provided in Fig. 4. The key parameters *i.e.*, peak shear strength and displacement, stiffness, 80 % post-peak shear strength and displacement, strain energy and failure mode from all the conducted tests (12 in total) are listed in Table 2. Fig. 4 shows that shear strength and stiffness for screws connecting CP-to-CFS assembly are greater than screws connecting OSB-to-CFS assembly. The loaded edge distance is not influential in determining the shear strength and stiffness of the tested specimens. This was mainly due to the fact that the minimum loaded edge distance (10.25 mm) was enough to prevent tear out of the sheathing edge.

Conversion of the full test results, on six screws, to single screw values is carried out by assuming the total peak shear strength of F_{max} and the peak shear strength of the individual screw F_{max-i} is equal to $F_{max}/6$. Assuming that all displacements occur at the screw locations implies that the displacement at the screw, Δ_i, is determined from the total displacement, as Δ_i equal to Δ [32]. Backbone curves for OSB- and CP-to-CFS screw shear behaviour have been derived based on the mean of the values listed in Table 2 to feed into the finite element (FE) models

Table 3
Tensile coupon test results.

Specimen	Base metal thickness t (mm)	Gauge length elongation ΔL_g (%)	Yield stress[a] $F_{y,0.2}$ (MPa)	Yield stress[b] $F_{y, auto}$ (MPa)	Upper yield stress $F_{y, upper}$ (MPa)	Tensile strength F_u (MPa)	Strain at tensile strength ε_u (mm/ mm)	Strain at rupture ε_r (mm/mm)
C100-41.3–1.6-W1	1.55	14.68	492.9	492.8	493.4	516.5	0.0725	>0.12
C100-41.3–1.6-W2	1.55	9.27	478.4	477.9	478.7	501.2	0.0673	>0.10
C100-41.3–1.6-F1	1.57	11.06	472.4	471.8	472.5	495.8	0.0641	>0.10
C100-41.3–1.6-F2	1.57	11.67	445.9	445.6	446.3	468.3	0.0579	>0.09
Mean	1.56		472.4	472.0	472.7	495.5		
STDEV	0.01		19.65	19.70	19.68	20.11		

[a] The 0.2% offset method is used here;

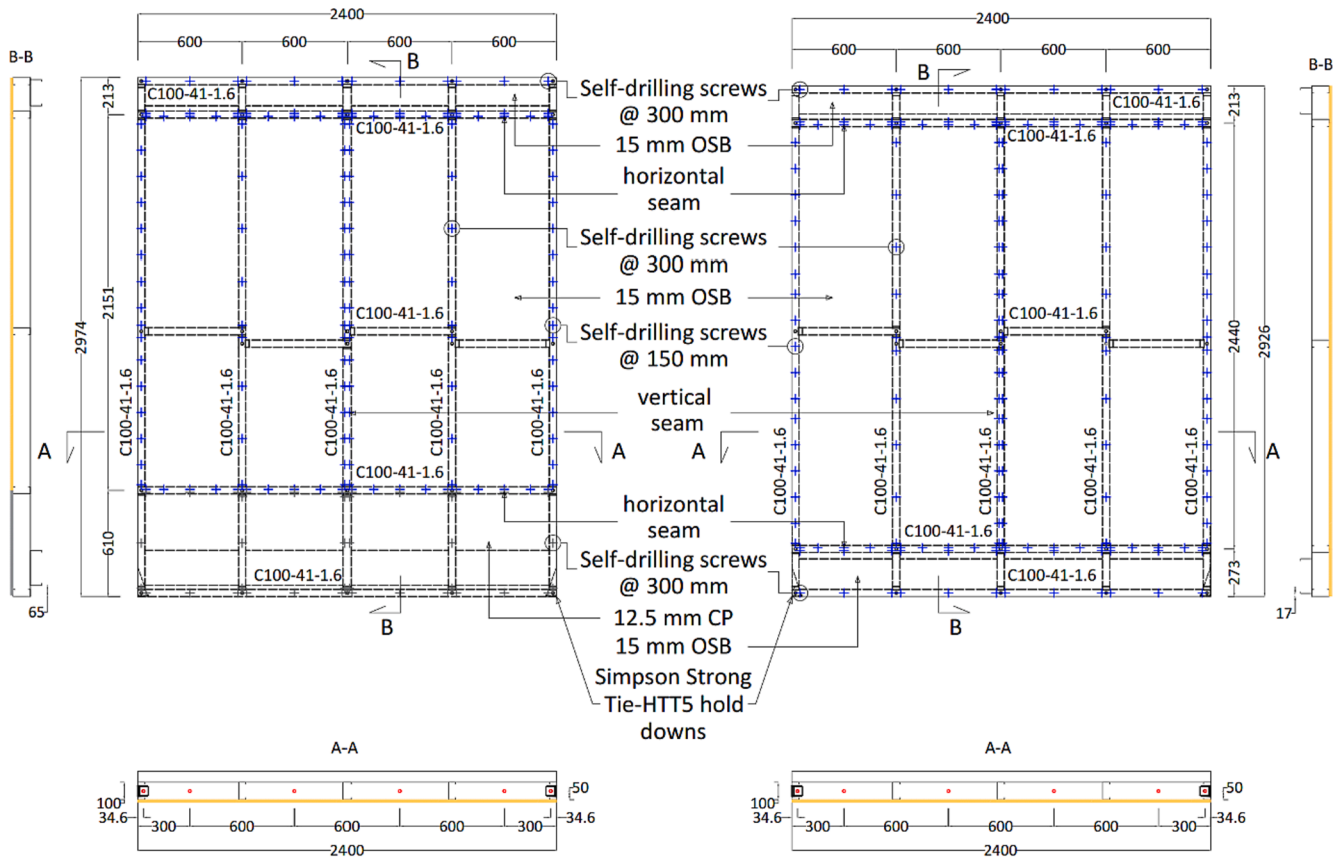[b] The autographic method used was the averaging of the stress levels at the 0.4% and 0.8% offset intercepts.

Fig. 8. Ground floor (left) and first floor (right) shear wall configurations.

Fig. 9. Test setup.

described in Section 4.2. It is worth noting that ECCS N. 124 (2009) [35] and ECCS N. 127 (2009) [36] could be followed for, respectively, testing of connections with mechanical fasteners in steel sheeting/sections and testing/design of fastenings for sandwich panels.

Table 4
Shear wall test results.

Shear wall ID	Test #	Peak lateral resistance (kN)	Disp. at peak lateral resistance (mm)	Stiffness (kN/mm)
GF	1	43.73	30.94	NA*
	2	43.17	40.68	2.06
	3	39.46	41.80	1.80
FF	1	69.21	49.92	NA*
	2	60.92	59.86	1.93
	3	64.04	57.24	1.79

* The peak resistance achieved was 20% greater than the estimated value so the result was disregarded as per BS EN 594:1996 [33].

3. Material property

To quantify the material properties of the CFS profiles used in the test specimens described in Sections 2 and 4, a series of 32 tensile tests were performed on coupons cuts longitudinally from the webs and flanges of C-section profiles. Fig. 5 shows the locations of the coupons. Testing was completed in accordance with BS EN ISO 6892–1 (2016) [37].

Uncoated steel thickness can be measured by removing the zinc coating. Therefore, both ends of all coupons were put in a 1 M HCl solution until the coating was removed. Fig. 6 shows the BS EN ISOdictated coupon dimensions for steel sheet thickness (1.6 mm) used in the tests. Yield (at 0.2 % offset) and ultimate tensile strengths for the C100-41.3–1.6 section were recorded with a mean of 472.4 MPa and 495.5 MPa, respectively. All yield stress values are considerably above the nominal 450.0 MPa except for F2 coupon. Young's modulus was not estimated from the linear data in the test results and is assumed to be 203400 MPa as prescribed in Eurocode 3 Part 1.3 [38].

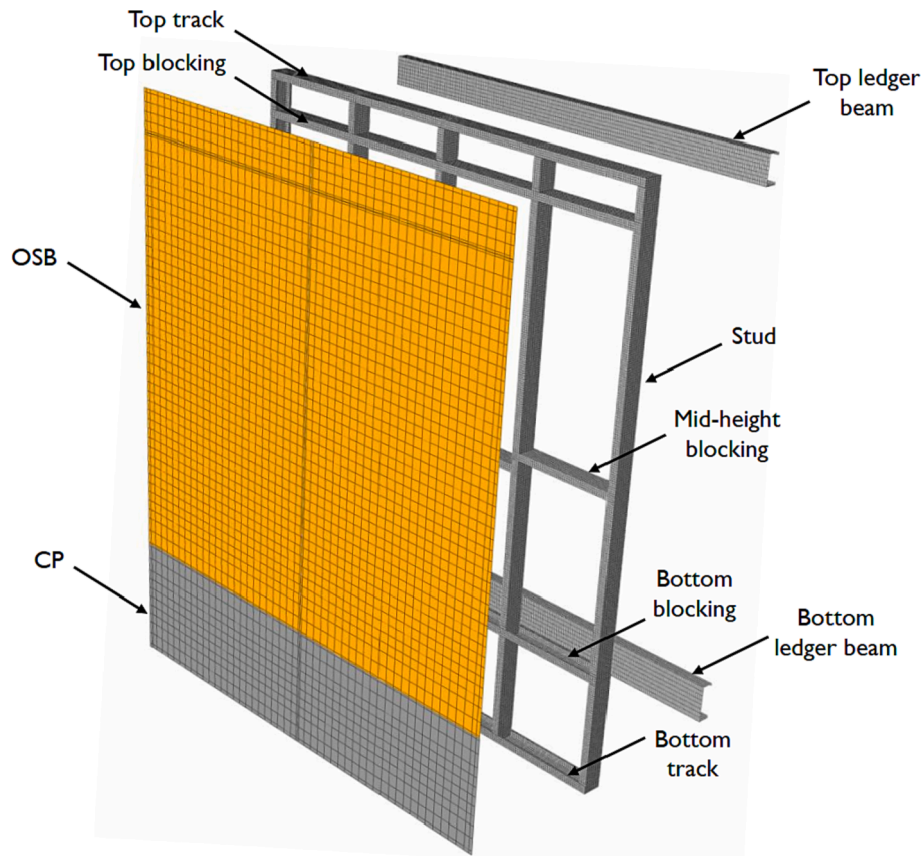Complete stress–strain curve for F1 coupon is plotted in Fig. 7, and

Fig. 10. Modelling of sheathing boards (OSB and CP) and CFS frame members (studs, tracks, blockings and ledger beams).
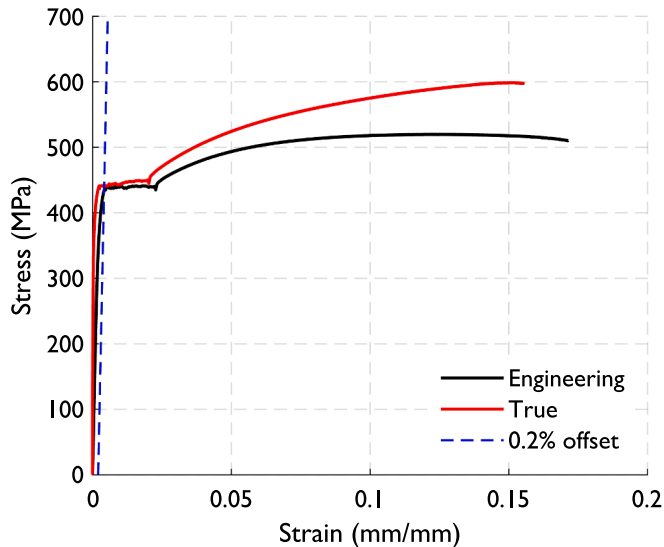

Fig. 11. Stress vs strain of the C100-41.3–1.6-F1 coupon.

Table 5
Plastic material parameters used for the nonlinear CFS material model in ABAQUS.

C100-41.3–1.6-F1 Coupon	
Stress (MPa)	**Strain (mm/mm)**
472.4	0.000
476.2	0.001
476.5	0.002
477.1	0.007
478.0	0.012
483.7	0.017
487.9	0.027
508.2	0.037
524.6	0.047
538.9	0.057
551.6	0.067
563.5	0.077
571.1	0.087
575.6	0.097
583.4	0.107
589.9	0.117
592.2	0.127
595.7	0.137
597.9	0.147
597.5	0.157

Table 3 summarizes the basic material properties: yield stress, ultimate stress, and maximum ductility.

4. Description of prototype shear walls and modelling protocol

4.1. Testing of CFS framed shear walls

A total of 6 shear wall tests (3 for each of the two wall typologies shown in Fig. 8), using a monotonic, displacement-controlled lateral loading protocol (BS EN 594: 1996 [33]), were completed to study the effect of: *i)* the presence of two ledger beams (*i.e.*, floor and ceiling ledger beams) on the interior face of the shear walls, *ii)* sheathing boards having different sizes from the overall shear wall and thus the presence of both vertical and horizontal seams in the shear wall, *iii)* use of CP board at the bottom stripe of the shear wall and *iv)* different screw spacing in the top and bottom stripes from the middle part of the shear wall. A detailed description of this test campaign is available in [31].
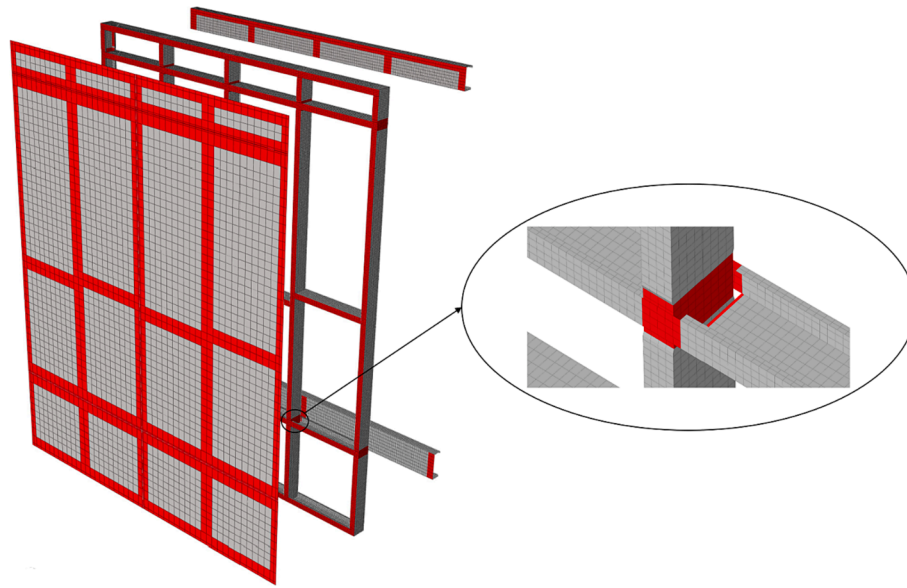
Fig. 12. Surface-to-surface contact between different shear wall components.
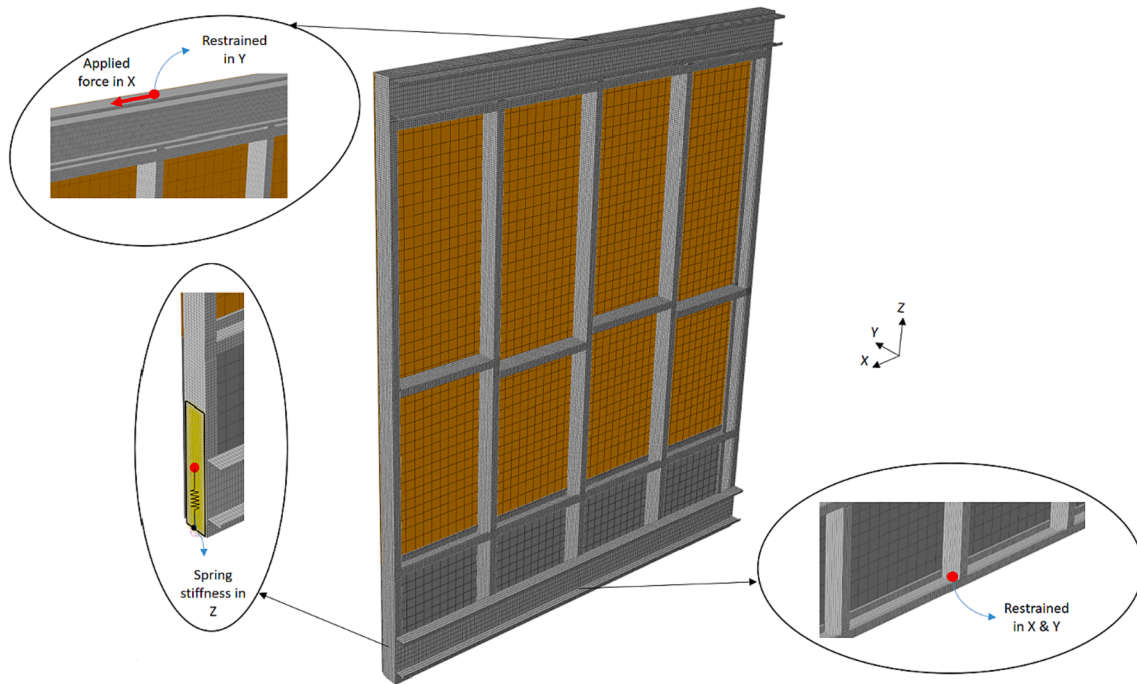

Fig. 13. Modelled boundary conditions.

Studs, tracks and blockings were lipped channel C100-41.3–1.6 with nominal grade of 450 MPa. Studs are spaced at 600 mm on centers. The C100-41.3–1.6 section has the following out-to-out nominal dimensions: a web depth of 100 mm, a flange width of 41.3 mm, a lip length of 11 mm, and a thickness of 1.60 mm. Ledger beams were realized with C200-65–1.6 and C150-65–1.6 for, respectively, floor and ceiling cassettes with nominal grade of 450 MPa. The C200/C150-65 1.6 have the following out-to-out nominal dimensions: a web depth of 200/150 mm, a flange width of 65 mm, a lip length of 13 mm, and a thickness of 1.6 mm. Sheathing boards on one side only, vertically oriented (strength axis or face grain parallel to studs), consisting of 15 mm OSB. In addition, 12.5 mm CP boards are used in the bottom stripe of the ground floor (GF) wall (see Fig. 8 left), with 10 mm offset from the base up to 610 mm high. Screw fixings are used to connect the studs to tracks/

blockings. Self-drilling screws are used to attach the OSB sheathing to the steel frame. Screw spacing around the edge of the sheathing boards is 150 mm. Field screw spacing is 300 mm (see Fig. 8). The screw spacing on the top and bottom stripes of the ground and first floor (FF) walls is 300 mm (see Fig. 8). Self-drilling screws are used to attach the CP boards on the bottom stripe of the GF wall to steel frame. The screw spacing on the bottom stripe of the GF wall is 300 mm (see Fig. 8). Simpson Strong-Tie HTT5 hold-down with 26 4.8 mm diameter 16 mm long screws is located at the bottom corners of each wall, to prevent uplift, and is connected to the base by a 16 mm diameter 60 mm long anchor bolt. The same type of bolts are used for shear anchors where their locations are shown in Fig. 8 (in red).

The tests setup (Fig. 9) and loading protocol were defined in agreement to BS EN 594 (1996) [33], which at the present is adopted in UK for
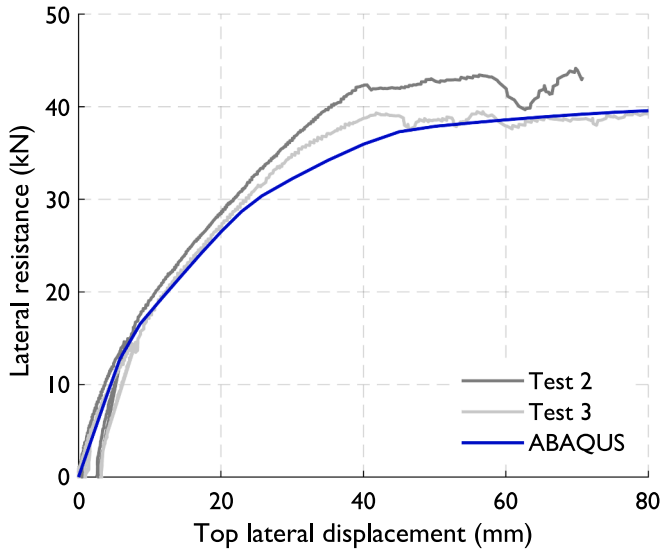
Fig. 14. Comparison between numerical and test results for the GF shear wall.

any wall test on both wooden frames and CFS frames.

The results of the above-described tests are summarized in Table 4.

4.2. Nonlinear FE modelling of CFS framed shear walls

The commercial FE software ABAQUS/CAE 2017 [39] was used to simulate the behaviour above-described CFS shear walls under lateral load. Fig. 10 shows the shear wall components as modelled. The following sections outline the element type and mesh generation, material model, contact modelling, screws modelling as well as boundary and loading conditions.

4.2.1. Element type and mesh generation

The nine-node shell element S9R5 with a reduced integration scheme (5 integration points through the thickness) was used to model all the CFS frame members (*i.e.*, studs, tracks, blockings and ledger beams). Schafer et al. (2010) [40] studied the sensitivity to element choice and mesh type in the computational modelling of CFS members and demonstrated that mesh density has a significant impact on the response of CFS members in FE analyses. Therefore, elements are placed every 5 mm along the longitudinal and transverse axes of each frame member. The four-node shell element S4R with a reduced integration was adopted to model the sheathing boards having a size of 50 mm with a height-to-width aspect ratio equal to 1:1. However, around the edges of the sheathing boards the element size was reduce to match the edge distances in the tested walls which are half and quarter the flange width (*i.e.*, 20.5 and 10.25 mm). The same strategy for selecting element types was adopted in [41].

4.2.2. Material properties

The CFS material properties are derived from the coupon tensile test results presented in Section 3. Fig. 11 shows the engineering and true stress–strain curves of the tensile test performed on C100-41.3–1.6-F1 coupon. In order to take into account the changes in the initial cross-section and length of the coupon in the plastic region (known as the necking phenomenon), conversions to true stress and true plastic strain were determined using Eq. (1) and (2).

$$\sigma = s(1+e) \tag{1}$$

$$\varepsilon_{plastic} = ln(1+e) - \frac{\sigma}{E} \tag{2}$$

Where s and e refer to engineering stress and engineering strain,

respectively. E is the Young's modulus, and true stress and true strain are σ and ε, respectively. $\varepsilon_{plastic}$ is the true, plastic strain (without the elastic strain component, which is subtracted at each point). In ABAQUS, the true stress–strain curve is used as an input for a material model with a classical von Mises plasticity and isotropic hardening. Table 5 provides the set of 20 data points used in the ABAQUS analyses. It is worth mentioning that the elastic modulus is used up to 100 % of the 0.2 % offset stress that is yielding prior to F_y as given in Table 3, which is consistent with the findings in Schafer et al. (2010) [40].

In order to minimize diaphragm deformations in OSB and CP board, the sheathings are modelled as isotropic elastic with a large Young's modulus equal to 210000 MPa and a Poisson's ratio (v_s) equal to 0.3 in all the three dimensions.

4.2.3. Contact modelling

Fig. 12 shows the interactions between: the frame members and the sheathing boards, the studs flange and ledger beams web as well as between the blockings and studs (including the contact between the edges of the holes in the web of the top and bottom blockings and the web of the studs). Surface-to-surface contact using the finite-sliding tracking method was selected to define the interaction relationship. Friction was also modelled with a coefficient of friction equal to 0.3 (for sheathing-to-CFS) as per tests conducted by Koubek and Dedicova (2014) [42], and frictionless contact between CFS frame members was assumed.

In order to prevent the adjacent sheathing boards from penetrating into each other, the adjacent sheathing boards' edges along the horizontal seams were connected via nonlinear Spring2 elements in ABAQUS. These spring elements have infinite compressive stiffness and zero tensile stiffness to prevent boards overlap.

4.2.4. Screws modelling

For modelling the CFS-to-CFS screws, the nodes coinciding with the stud-to-track/blocking/ledger were constrained to have identical displacements in all the three dimensions using the mathematical constraints (*Equation keyword in ABAQUS). As for the sheathing-to-CFS screws modelling, the UEL subroutines developed by Chu Ding (2015) [43] were adopted. Calibrated Pinching4 model, based on the test results described in Section 2.3, is assigned to the UEL so that the nonlinear shear behaviour of the sheathing-to-CFS screws can be simulated with an acceptable accuracy. In order to consider changes in displacement trajectory, a radial spring is used in the UEL. This would avoid the overestimation of the shear strength and stiffness of the screw. It is worth mentioning that Spring2 element in ABAQUS can be used to simulate the screws (as adopted in [25]), however, the distance between the two nodes of this element should be less than the displacement in the first leg of the strength-displacement backbone curve assigned to this element. This cannot be achieved for CFS shear walls sheathed with wood- and/or CP-based boards of>10 mm thickness.

4.2.5. Model boundary conditions and solution algorithm

The shear wall under lateral load is expected to have in-plane displacements only. Therefore, to avoid any out-of-plane displacement, the top track of the tested walls was constrained with transverse roller, and all nodes on the web of the top track of the simulated walls were fixed in the transverse direction. The lateral load is applied at the top of the shear wall as displacement control. A displacement of 100 mm is assigned as a boundary condition at a reference point (RP) which is located at the center of gravity of the upper track. The RP is tied at one edge of the track cross section using the rigid body command in ABAQUS. The Newton-Raphson integration algorithm with artificial damping is used for solving the nonlinear equilibrium equations while considering the geometric nonlinearity. Moreover, the base of the wall has restrained horizontal translations, therefore, the bottom track is restrained at four nodes to replicate the effect of the shear anchors that connect the wall to the foundation. The anchor bolts connecting the bottom track to the
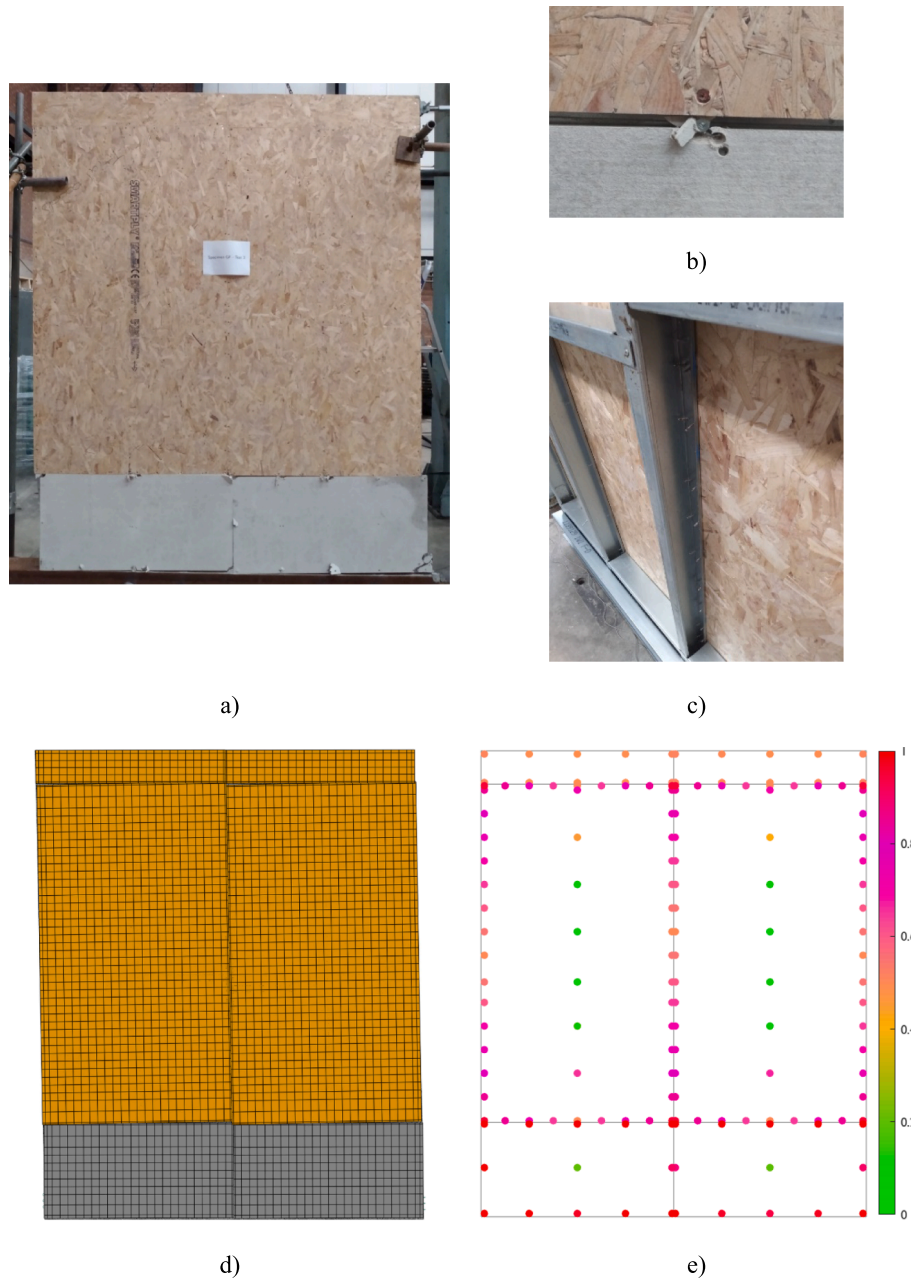
Fig. 15. a) Measured deformed shape, b) screw failure, c) screw tilting in studs, d) FE simulated deformed shape and e) Screw demand-to-capacity ratios at peak lateral resistance of GF-150–300 shear wall.

foundation are modelled as pinned connections by fixing the nodes that coincide with the anchor bolts location on the web of the bottom track in both horizontal and transverse direction. This allows force in the shear wall to be transferred directly to the foundation in these two directions. The modelling approach related to hold downs was adopted from [25] where all the nodes in the chord studs that are in contact with the hold down are tied to a rigid body using rigid body type tie constraints and linked to a fixed node on the ground in the vertical direction via Spring2 element as shown in Fig. 13.

4.3. Validation of the FE modelling protocol

A comparison between experimental and numerical results is presented in this section. In particular, Section 4.3a discusses the lateral behaviour including peak lateral resistance, top lateral displacement at peak resistance and initial stiffness. An insight into the failure mode of

the tested and simulated shear walls is provided in Section 4.3b.

a) Lateral behaviour.

Lateral resistance vs displacement curves of both experimental (dark and light grey) and numerical (blue) results are shown in Fig. 14. The results illustrate that the peak lateral resistance of the tested shear wall is accurately captured with 4 % difference from the mean of the two experimental peak lateral resistances ($F_{peak-exp}$ = 41.32 kN vs $F_{peak-num}$ = 39.51 kN). The displacement corresponding to the peak lateral resistance differs by 6 % from the mean of the two displacements obtained from the experimental tests ($d_{peak-exp}$ = 75.41 mm vs $d_{peak-num}$ = 80.03 mm). The initial stiffness obtained via numerical simulation is in agreement with its experimental counterpart (1.93 vs 1.83 kN/mm). Furthermore, the trend of the numerical results in terms of lateral resistance vs top lateral displacement, is similar to the test results including the post-peak behaviour where the tested and simulated shear walls exhibits a ductile behaviour without a significant drop in lateral
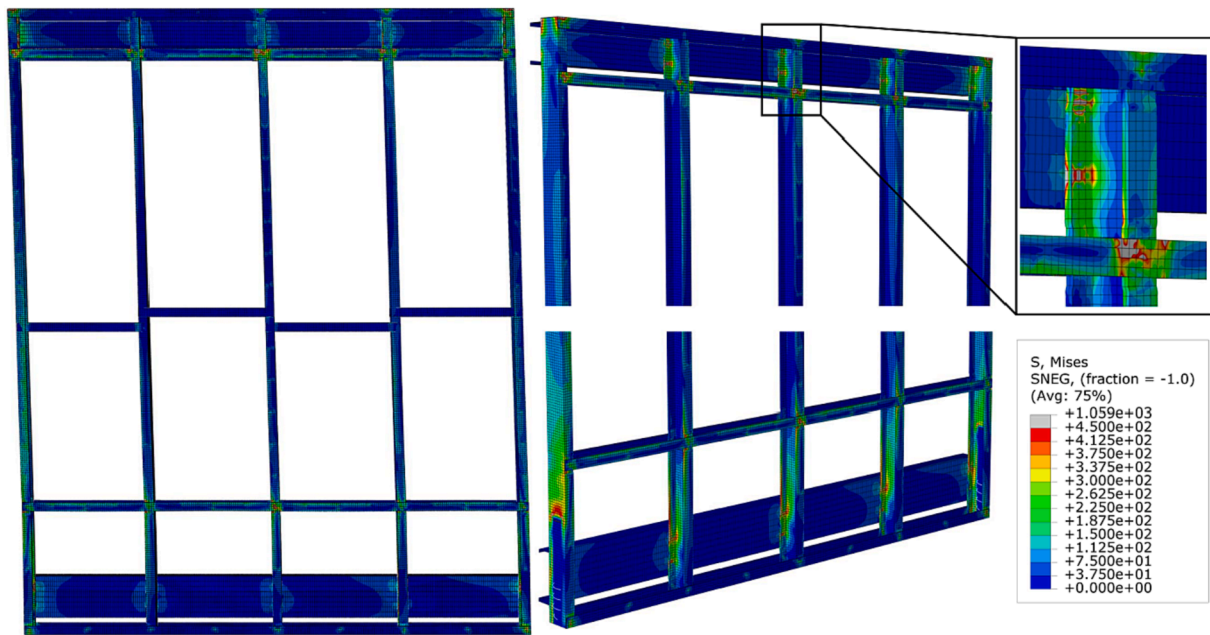
Fig. 16. Von Mises stress distribution in the GF shear wall at peak lateral displacement.
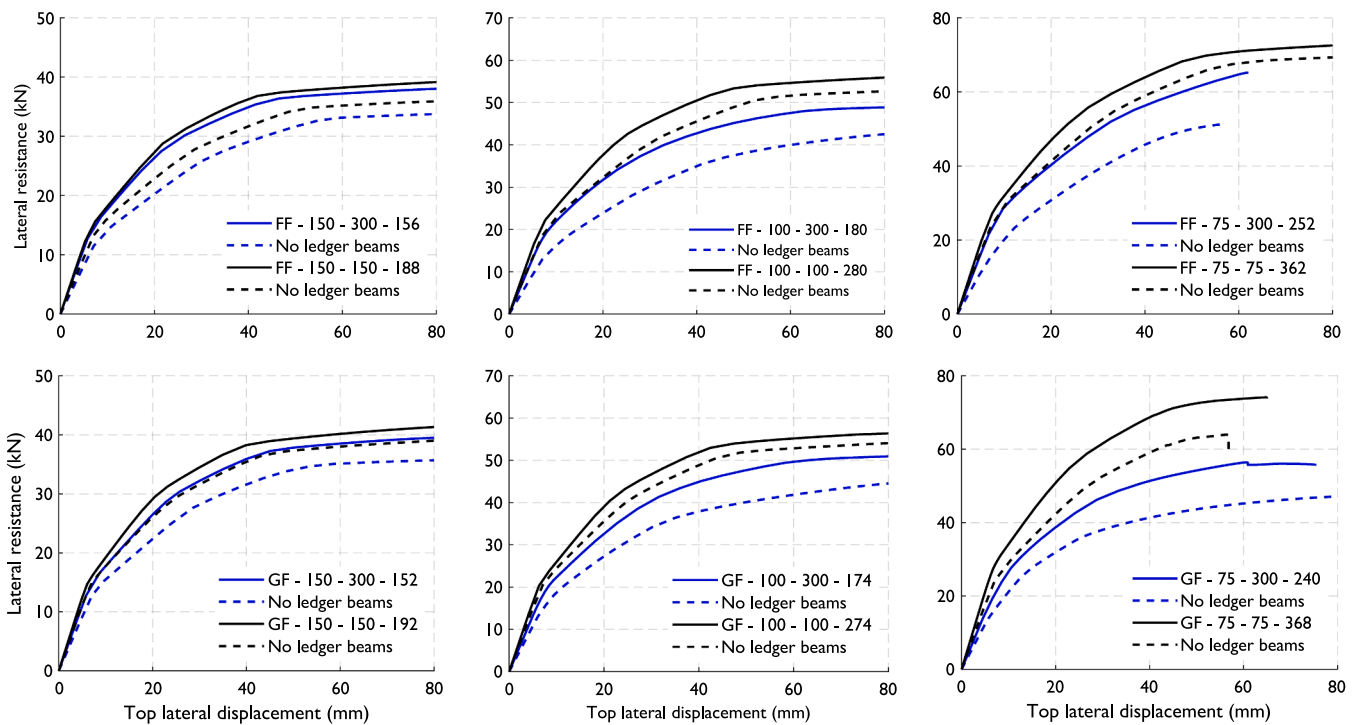

Fig. 17. Lateral resistance vs top lateral displacement curves considering ground and first floors (top and bottom subfigures, respectively), screw spacing (from left to right: 150, 100 and 75 mm) with and without ledger beams.

resistance for increasing displacements. In the other hand, the above mentioned differences are mainly due to the fact that all the sheathing-to-CFS screws were given the mean values of the results shown in Fig. 4, this resulted in a slightly underestimation of the stiffness at top lateral displacements>25 mm.

b) Failure mode.

Given the fact that, at low loading levels, sheathing-to-CFS screws are the main source of lateral resistance of CFS framed shear walls, the failure modes are represented by tilting and bearing of the screws. The failure started by cracking of the CP boards around the screws located near the corners until the parts surrounding those screws detached. This was mainly due to the fact that the CP-to-CFS screws exhibit a relatively stiffer shear behaviour compared to OSB-to-CFS screws (see Fig. 4), they were the first to fail in the tested GF shear walls. As the loading level increases, contact between framing elements contributes to the lateral resistance of the shear wall. Fig. 15 shows both experimental and numerical deformed shapes at the peak lateral resistance as well as the screws failure (tilting and edge distance failure). The demand-to-capacity ratio, shown in Fig. 15e, was defined as the ratio between the applied force on a given sheathing-to-CFS screw fastener and the peak
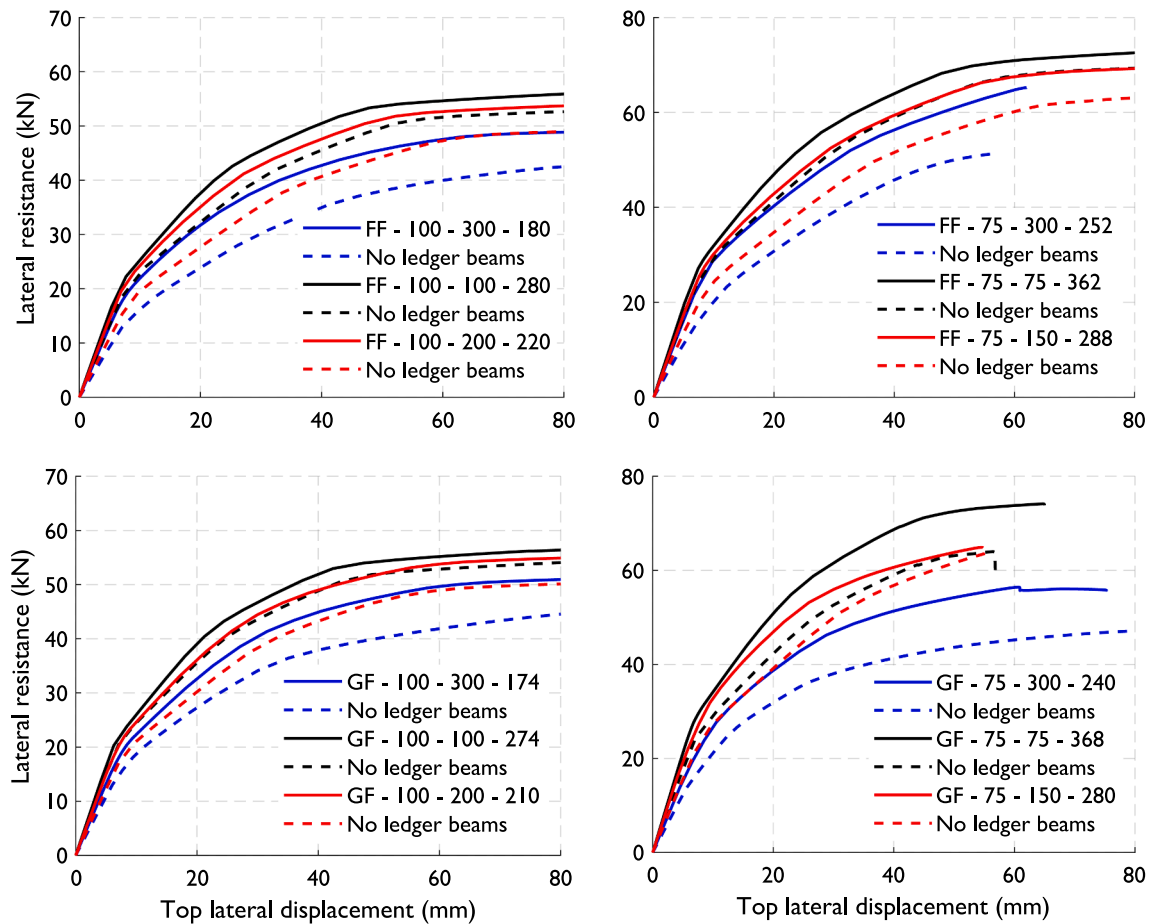
Fig. 18. Lateral resistance vs top lateral displacement curves considering screw spacing (from left to right: 100 and 75 mm) with and without ledger beams.

capacity of the connection itself to indicate the failed connections. It is clear that the sheathing boards exhibit a rigid rotation while the CFS frame show a deformed shape as a parallelogram and that a good agreement has been achieved between the numerical and experimental test results in terms of the position of the failed connections.

Von Mises stress contour is shown in Fig. 16. It is explicit that the regions surrounding CFS-to-CFS connections as well as the areas near the corners of the sheathing boards endured relatively high stress where the grey area represents the yielded steel. Moreover, Fig. 16 (left) shows some member curvature due to the presence of the top and bottom blockings and the floor and ceiling ledger beams.

5. Parametric study

Once the FE modelling protocol has been validated using experimental test results, it can be applied and extended to evaluate the lateral behaviour of other similar CFS framed shear walls. This work, in particular, aimed to study the effect of additional construction details which are commonly adopted in modular construction and go beyond the scope of available lateral design guidelines. The investigated details include: (i) presence of floor and ceiling ledger beams on the interior face of the shear wall, (ii) sheathing boards having different sizes from the overall shear wall and thus the presence of both vertical and horizontal seams, (iii) use of CP boards at the bottom stripe of the shear wall and (iv) different screw spacing in the top and bottom stripes from the middle part of the shear wall.

A total of 38 walls have been simulated and the results in terms of lateral resistance vs top lateral displacement curves are illustrated in Figs. 17 and 18. The peak lateral resistance and its corresponding displacement as well as the initial stiffness are listed in Table 6. The wall

naming convention utilized is summarized as follows: the first two characters, either GF (ground-floor) or FF (first-floor) corresponds to the floor level; the following number refers to the screw spacing at the middle part of the wall (see Fig. 8): either 150, 100 or 75; following this, the second number, either 300, 200 or 150 refers to the screw spacing at the top and bottom stripes of the wall, and the third number represents the total number of screws in the entire wall. For example, wall GF-150–300-152 is a ground-floor wall having 150 mm screw spacing at its middle part and 300 mm screw spacing at its top and bottom stripes with a total number of screws equal to 152.

a) Effect of floor and ceiling ledger beams.

Balloon framing is one of the structural features of the modular construction, thus the presence of floor and ceiling ledger beams as shown in Fig. 9. As shown in Figs. 17 and 18 (dotted vs solid lines) and listed in Table 6, the inclusion of ledger beams increases the peak lateral resistance by up to 27 % and the stiffness by up to 42 %. This is due to the fact that the floor and ceiling ledger beams create a portal action in the CFS frame which contributes to the global lateral behaviour (strength and stiffness) of the shear wall. Moreover, at a system level (i.e., full module), it is expected that the above percentages would be higher with the presence of the entire floor and ceiling components (i.e., joists and sheathing boards) as well as the presence of the perpendicular external walls.
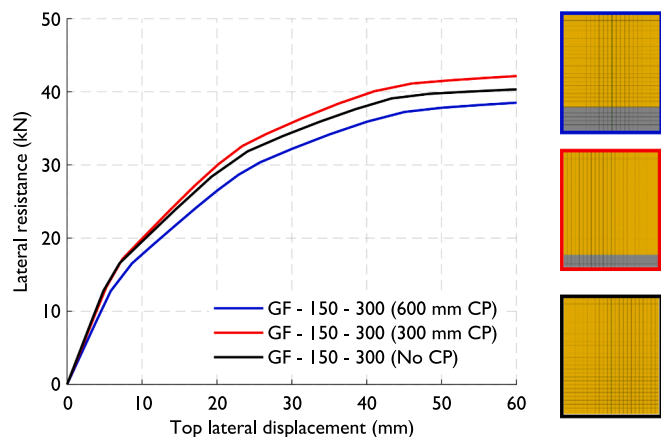
b) Effect of CP board height.

The presence of CP boards at the bottom stripe of the ground floor walls is driven by the need to meet the above ground level water proofing requirements in the UK. The effect of the CP board height on the lateral behaviour of the CFS framed shear wall is investigated in this section. Fig. 19 shows that the shear wall stiffens up as the height of the CP boards decreases to the point that having a CP board of 300 mm

Table 6
Key CFS shear wall simulation results.

Floor level	Screw spacing (mm)	Total # of screws	Floor and ceiling ledger beams	Peak lateral resistance (kN)	Top disp. at peak lateral resistance (mm)	Stiffness (kN/mm)
Ground floor	75/75	368	✓	74.13	64.77	3.92
			–	63.97	56.48	3.38
	75/150	280	✓	64.86	54.61	3.38
			–	63.87	56.01	2.65
	75/300	240	✓	56.40	60.68	2.62
			–	47.34	83.70	2.11
	100/100	274	✓	56.34	79.07	2.68
			–	54.06	79.92	3.05
	100/200	210	✓	54.92	80.70	2.74
			–	50.07	78.55	2.08
	100/300	174	✓	50.96	80.50	2.41
			–	44.56	80.14	1.89
	150/150	192	✓	41.32	79.92	2.28
			–	38.93	78.31	1.89
	150/300	152	✓	39.51	80.03	1.83
			–	35.66	78.55	1.48
	150/300[a]	150	✓	43.21	81.01	2.34
			–	33.99	77.78	1.92
	150/300[b]	140	✓	41.01	78.31	2.34
			–	34.06	82.28	1.92
	150/300[c]	147	✓	NA[d]		
			–			
First floor	75/75	362	✓	72.49	78.98	3.51
			–	69.41	81.92	2.55
	75/150	288	✓	69.14	78.03	3.27
			–	63.03	79.39	2.49
	75/300	252	✓	65.24	61.99	2.68
			–	51.35	56.82	2.13
	100/100	280	✓	55.78	77.89	2.89
			–	52.73	82.28	2.97
	100/200	220	✓	53.80	82.14	2.35
			–	48.91	78.55	2.03
	100/300	180	✓	48.80	77.98	2.42
			–	42.49	79.86	1.77
	150/150	192	✓	39.25	81.95	2.13
			–	35.88	78.55	2.02
	150/300	156	✓	38.09	81.48	1.76
			–	33.77	79.88	1.24

[a] GF-150–300-150 with 300 mm CP board in the bottom stripe (see Fig. 21c);
[b] GF-150–300-140 with no CP board in the bottom stripe (see Fig. 21d);
[c] GF-150–300-147 with top and bottom stripes sheathed with one 2400 mm wide board (see Fig. 20);
[d] No complete results were obtained for this shear wall as explained in Section 5c.

Fig. 19. Lateral resistance vs top lateral displacement curves considering three heights of CP boards.

height results in the optimum lateral behaviour. Reducing the height of the sheathing in the bottom stripe turned out to be structurally beneficial and stiffens up the shear wall as it reduces the soft-story effect witnessed in the case of shear walls with CP boards of 600 mm height.

This is mainly due to the fact that the deformed shape of the sheathing board is a rigid rotation, thus, the higher the height-to-width aspect ratio, the more screws are actioned to withstand lateral loads. By reducing the height of the CP boards to be at the same level as that of the floor, the height-to-width aspect ratio of the sheathing boards in the middle part of the shear wall allows for the best mechanism of resisting lateral loads.

c) Effect of sheathing layout in the top and bottom stripes.

The sheathing width throughout the height of the shear wall should be consistent in order to allow a proper rotation of the boards, which in turn actions as many screws as possible to provide lateral resistance. An analysis of a shear wall with the sheathing layout as shown in Fig. 20 was prematurely terminated due to convergence issues. This was mainly due to the high width-to-height aspect ratio of the sheathing boards in the top and bottom stripes of the shear wall (>8 and 4, respectively) which in turn resulted in incompatibility in the deformed shapes of the sheathing boards in the different parts of the shear wall leading to a concentration of stresses. Although the sheathing layout shown in Fig. 20 has some benefits from a manufacturing point of view (*i.e.*, in terms number of cuts, boards waste and easiness of installation), this should be avoided in order to optimize the shear wall lateral behaviour.

d) Effect of screw density in top and bottom stripes.

For both GF and FF shear walls, a steady increase in the lateral resistance is associated with screw spacing reduction as illustrated in
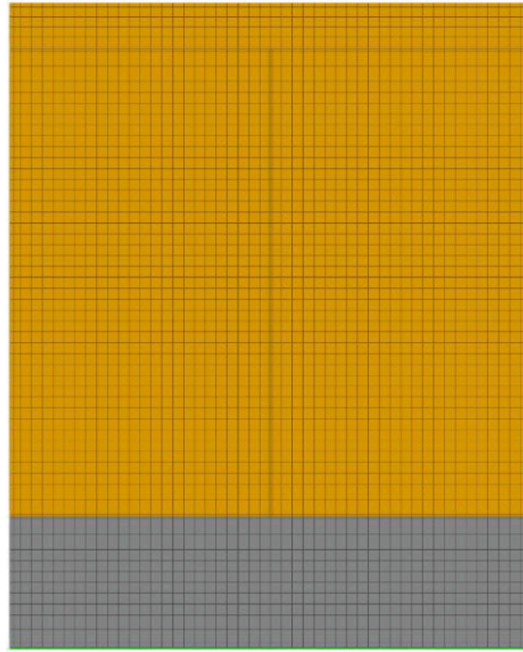
Fig. 20. Sheathing's layout to be avoided in CFS framed shear walls.

Figs. 17 and 18. For the case where the screw spacing is equal to 75 mm, the failure mode shifted from sheathing-to-CFS screws damage to local-distortional buckling of the compressed chord stud as shown in Fig. 21, which hampered the engagement of as many screws as possible to generate additional lateral resistance. Furthermore, it can be seen in Fig. 18 that doubling the screw spacing in the top and bottom stripes would results in a non-drastic drop in the lateral resistance of the shear wall with 3 % and 13 % as minimum and maximum, respectively.
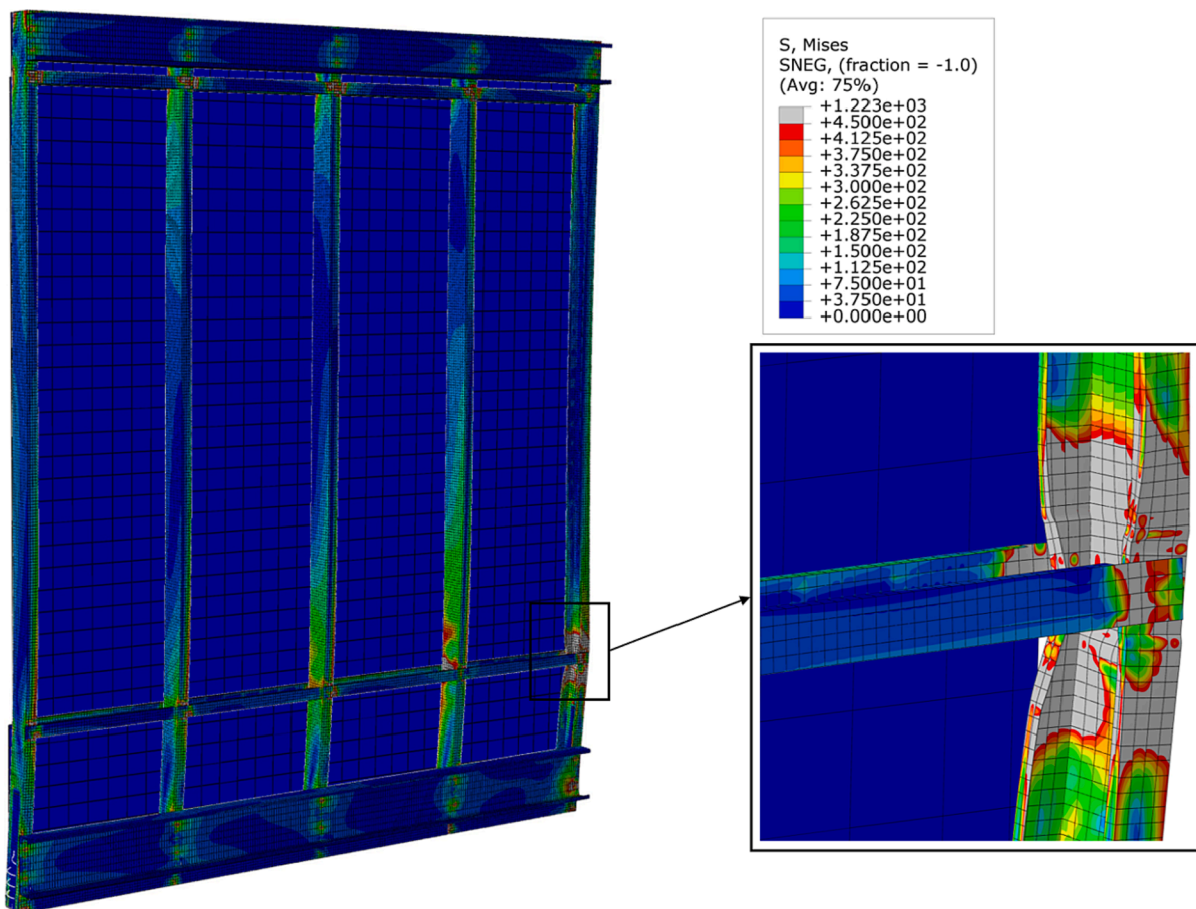

Fig. 21. Plastic hinge formation in the numerical model of GF-75–150-280.
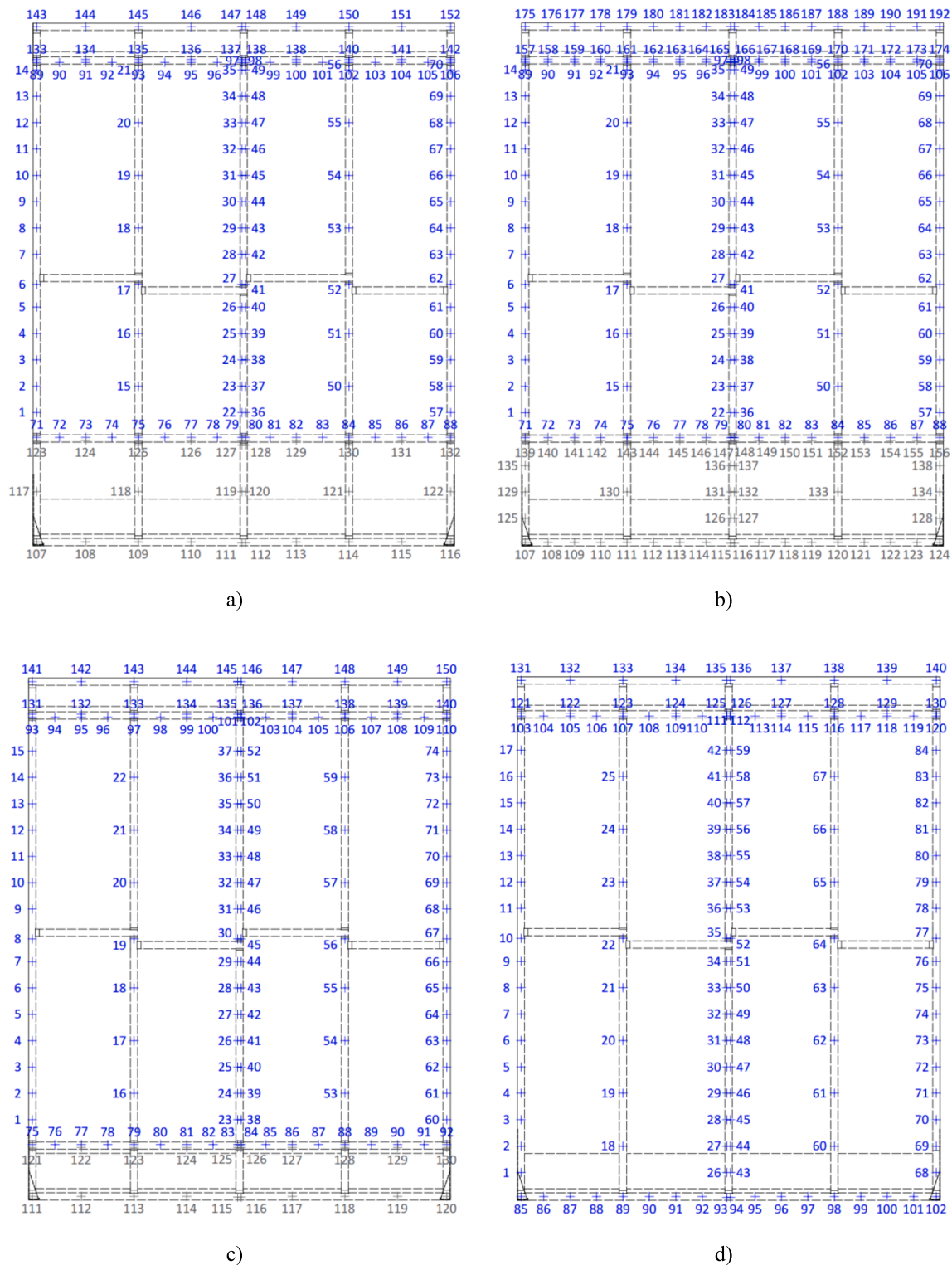
Fig. 22. Screws tag in: a) GF-150–300, b) GF-150–150, c) GF-150–300-300-CP and d) GF-150–300-No-CP shear walls.

6. Screw shear demand evaluation

One interesting feature of the UEL employed in this study is the ability of monitoring the output in terms of load-deformation curve as well as the angle between the screw and the global horizontal/vertical axis at all levels of lateral displacements of the shear wall. This relies on the UEL subroutine itself to feed specific data into a text file. A Matlab [44] script was developed to extract results from a text file that the UEL subroutine outputs for each element (i.e., screw) and post-process those results to generate meaningful plots. It is worth noting that, to the authors' knowledge, these data cannot be measured via physical testing.

In this section, the above-described feature of the UEL subroutine is explored. Fig. 22 shows the screws location with their tag in GF-150–300, GF-150–150, GF-150–300-300-CP and GF-150–300-No-CP shear walls. Figs. 23-26 show the load-deformation curve, percentage of usage, failure of every single screw up to the peak lateral resistance of
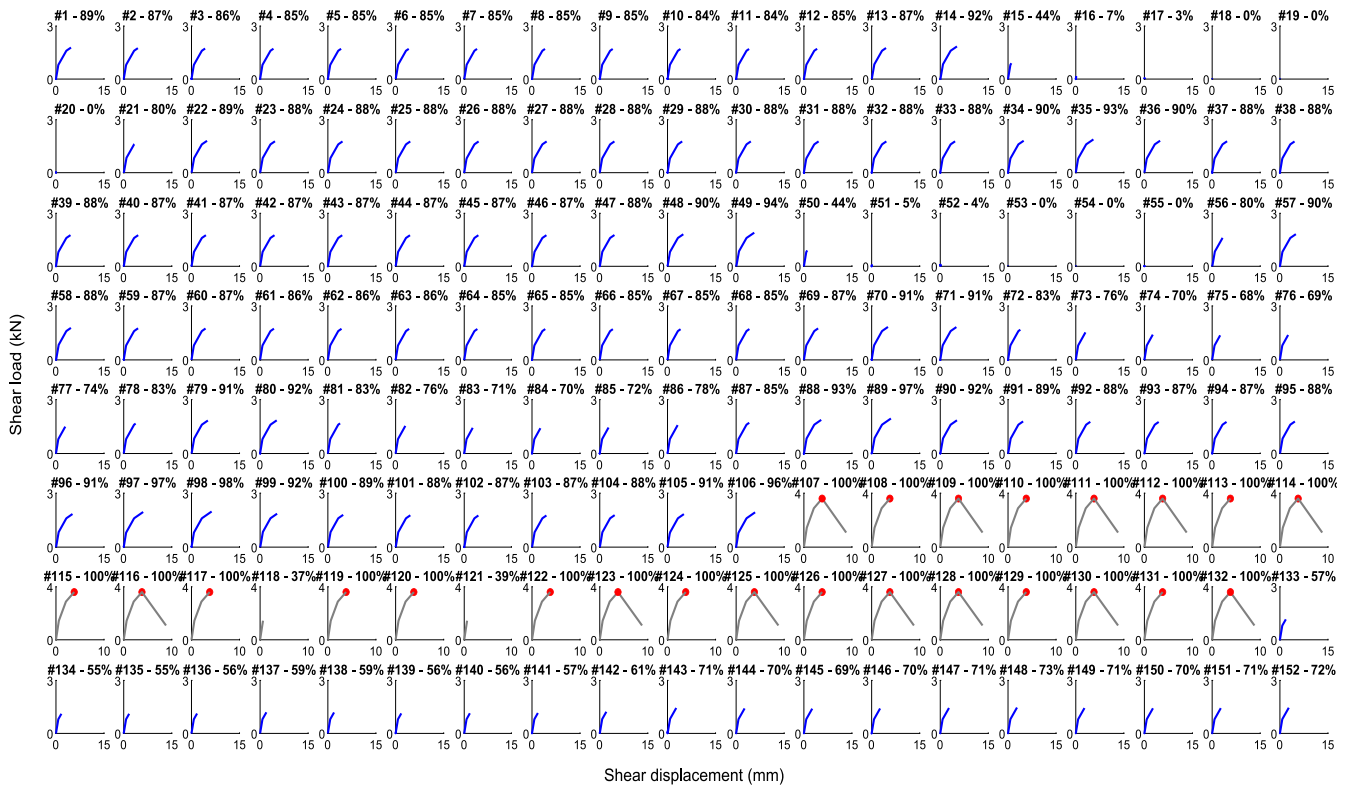
Fig. 23. Shear load–displacement curve, percentage of usage and failure occurrence of the GF-150–300 shear wall sheathing-to-CFS screws.
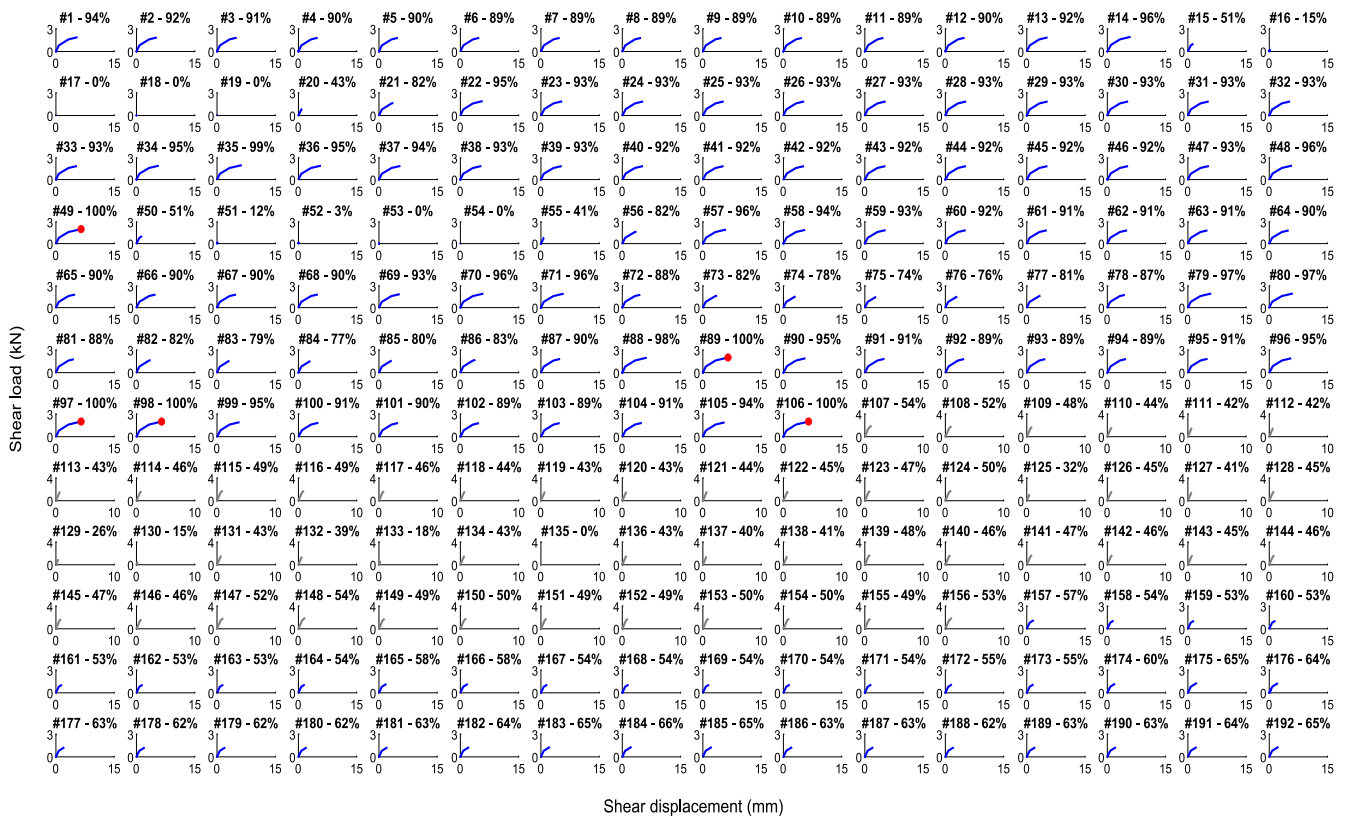

Fig. 24. Shear load–displacement curve, percentage of usage and failure occurrence of the GF-150–150 shear wall sheathing-to-CFS screws.
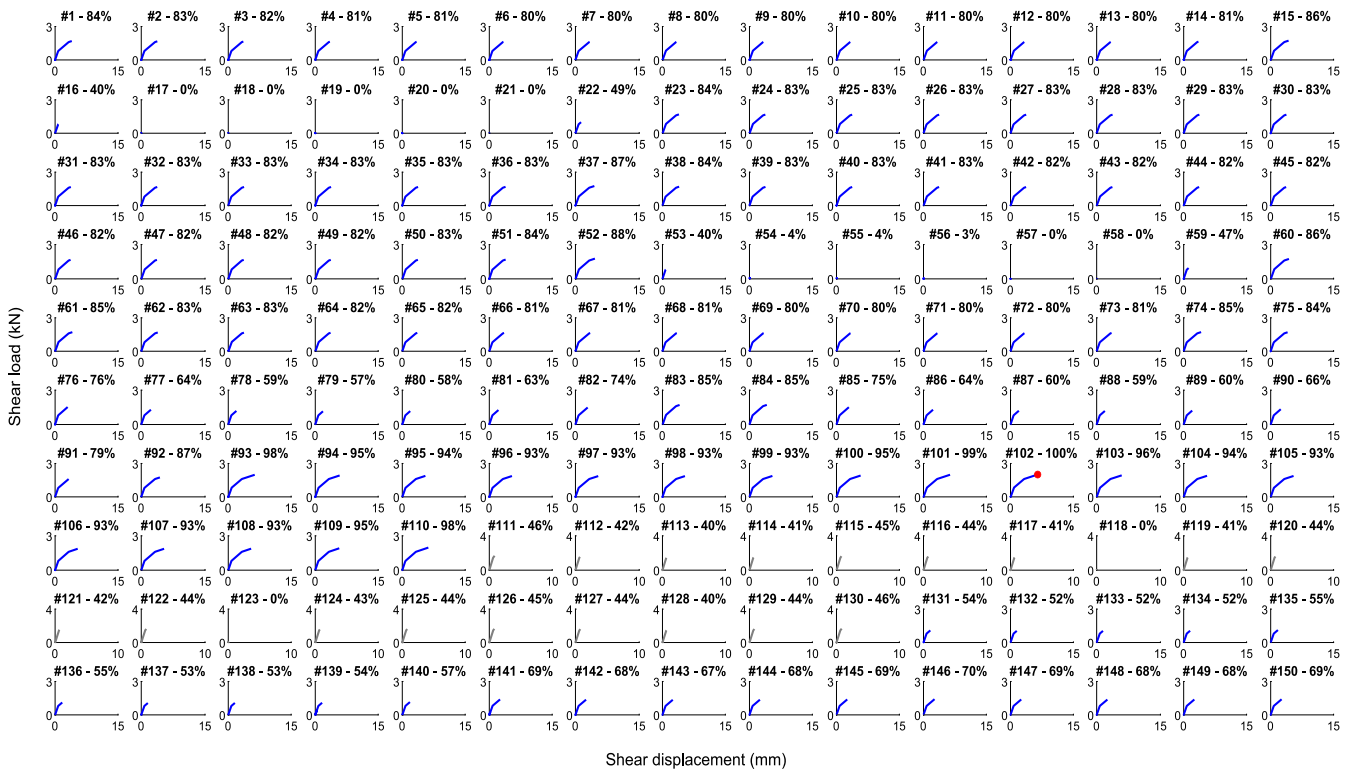
Fig. 25. Shear load–displacement curve, percentage of usage and failure occurrence of the GF-150–300-300-CP shear wall sheathing-to-CFS screws.
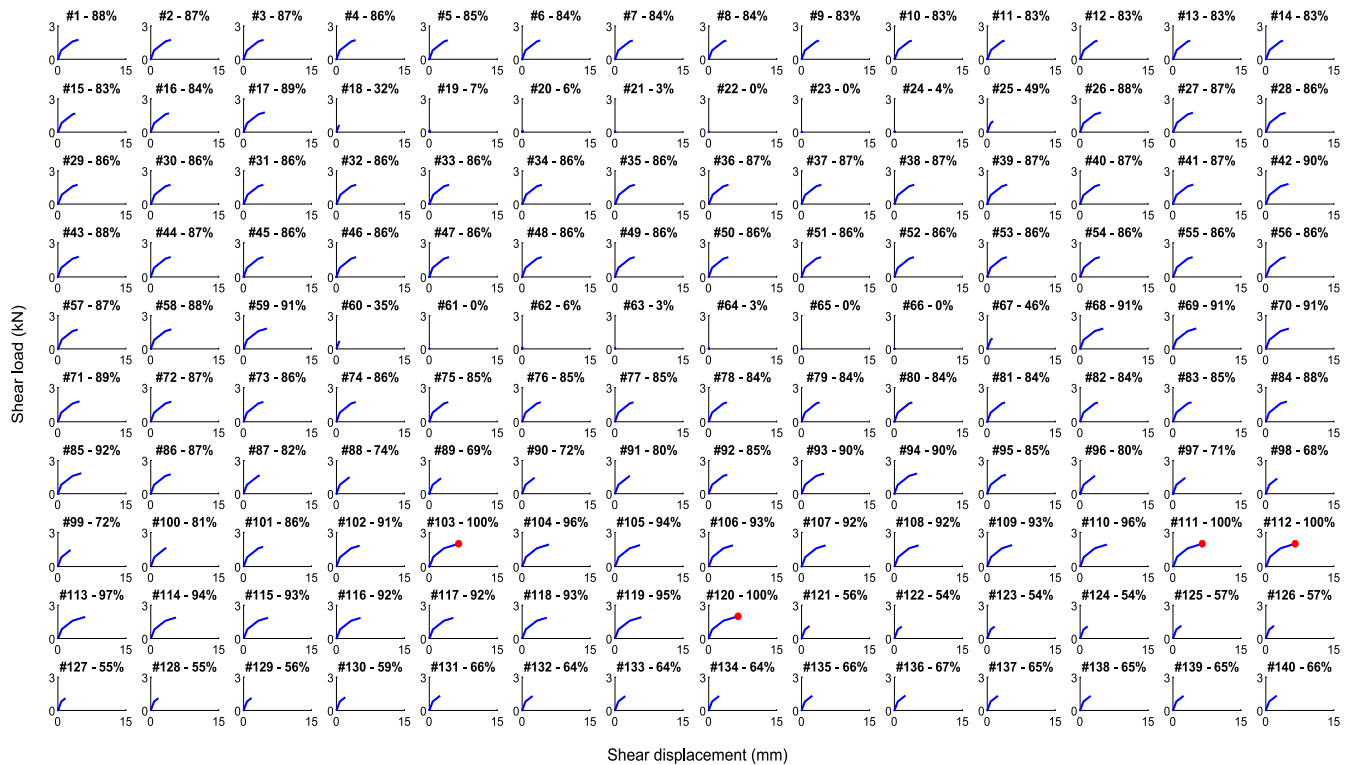

Fig. 26. Shear load–displacement curve, percentage of usage and failure occurrence of the GF-150–300-No-CP shear wall sheathing-to-CFS screws.

the analyzed shear walls. Comparing the results shown in Figs. 23 and 24, it can be seen that more uniform distribution of shear demand is noticed in GF-150–300 shear wall than in GF-150–150 shear wall. This is due to the fact that less screw density in the top and bottom stripes have

made an effective use of the screws in those parts of the shear wall. The same set of information can give insight into the sheathing layout that makes it easy for the screws to engage in resisting the lateral load applied on the shear wall. Figs. 23, 25 and 26, which correspond to shear
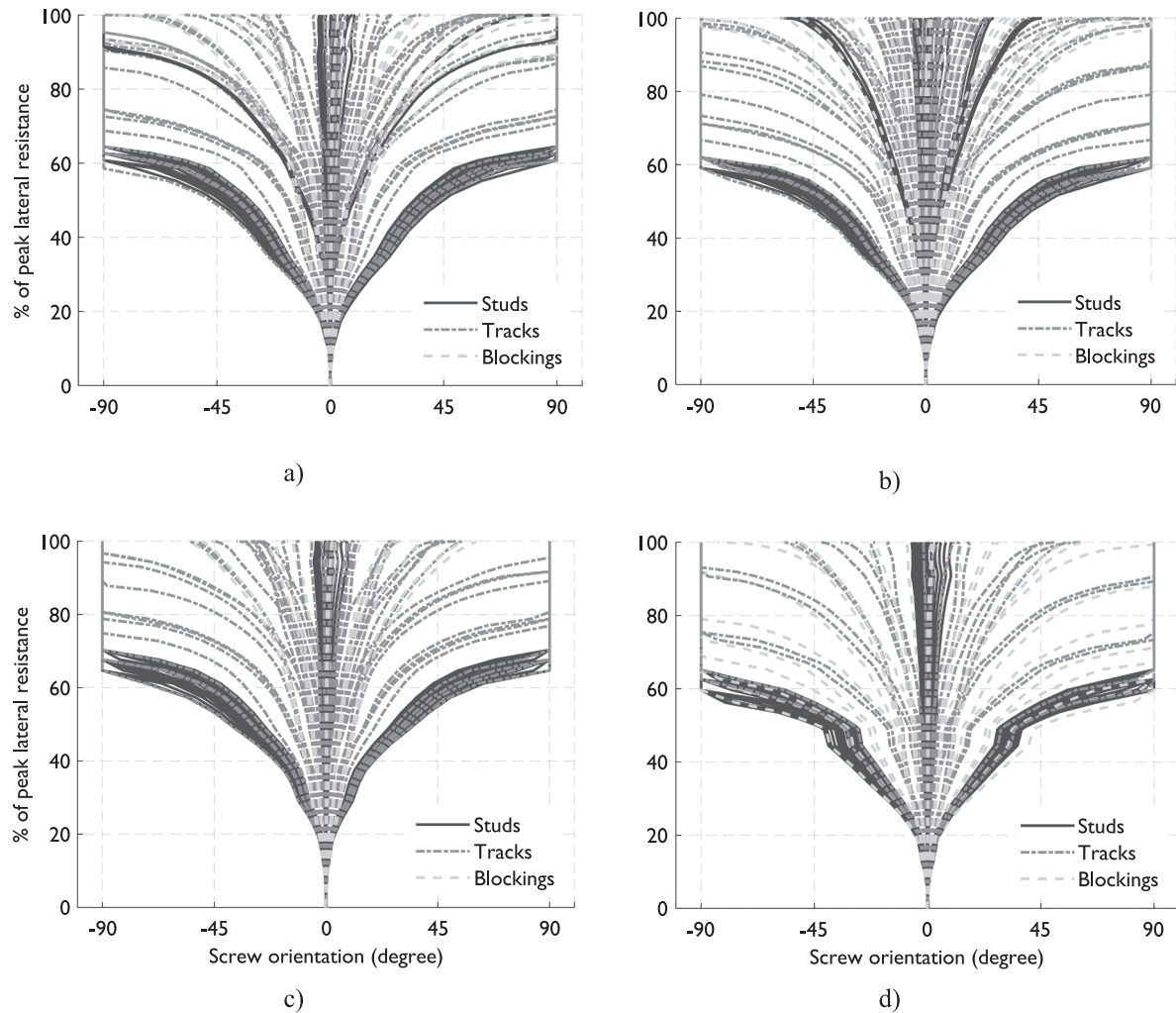
Fig. 27. Orientation of the screws vs peak lateral resistance percentage of: (a) GF-150–300, (b) GF-150–150, (c) GF-150–300-300-CP and (d) GF-150–300-No-CP.

walls with 600 mm, 300 mm and 0 mm CP board in its bottom stripe, show the different trend of screw shear demand where a more uniform distribution of screw shear load is witness in GF-150–300-300-CP and GF-150–300-No-CP shear walls which in turn confirms the results shown in Fig. 19.

Fig. 27 shows that the orientation of the sheathing-to-CFS screws changes throughout different levels of lateral demand on the shear wall (up to the peak lateral resistance). The figure shows that the screw load is vertical along most of the studs height, but near the sheathing corners the load is oriented diagonally. A similar trend is observed for the screws connecting the sheathing boards to horizontal frame members (tracks and blockings).

7. Comparison with design codes

In this section, results of the above-described numerical simulations are compared, where relevant, to test results provided in AISI S400 [4] and results of the semi-analytical method described in the Steel Construction Institute (SCI) publication ED002 [45]. Table 7 shows the differences in terms of the peak lateral resistance obtained from ABAQUS simulation, AISI S400 and ED002. The comparison shows that the design codes underestimate the peak lateral resistance of the shear wall with a maximum of 23 %. This highlights the need for full scale tests to assist the lateral design of CFS structures as well as the need for advance numerical simulation protocols for the development of CFS shear wall

typologies that go beyond the scope of the current lateral design codes for CFS structures.

8. Conclusions

Despite many experimental and numerical studies have been performed to understand the behaviour of CFS framed shear walls subjected to monotonic and cyclic lateral loads, the effect of modular construction details on lateral behaviour of CFS framed shear walls has not been investigated yet. Therefore, this paper, first presents a shell FE modelling protocol that has been developed in ABAQUS and includes material and geometric nonlinearities as well as contact model with friction. The modelling approach could be adopted in the future for the study of similar wall systems. In particular, in the presented model, the sheathing-to-CFS screws were modelled using UEL subroutines capable of reproducing, as accurately as possible, the screw strength and stiffness degradation under monotonic load. This modelling protocol has been validated based on experimental tests carried out by the authors, as part of a knowledge transfer partnership (KTP) project between the University of Leeds and ilke Homes ltd., where a good agreement (with about 4 % difference) has been achieved between the experimental and numerical results.

Second, this paper discusses the effect of modular construction details on the behaviour of laterally-loaded CFS shear walls. In particular, the relevant construction details include: *(i)* presence of floor and ceiling

Table 7

Shear wall lateral strength comparison between ABAQUS model, SCI ED002 and AISI S400 design codes.

Floor level	Screw spacing (mm)	Floor and ceiling ledger beams	FE (kN)	SCI ED002 (kN)	Difference (%)	AISI S400 (kN)	Difference (%)
Ground floor	75/75	✓	74.13	63.2	1	61.67	4
		–	63.97				
	75/150	✓	64.86				
		–	63.87				
	75/300	✓	56.4				
		–	47.34				
	100/100	✓	56.34	47.4	14	49.39	9
		–	54.06				
	100/200	✓	54.92				
		–	50.07				
	100/300	✓	50.96				
		–	44.56				
	150/150	✓	41.32	31.6	23	32.93	18
		–	38.93				
	150/300	✓	39.51				
		–	35.66				
First floor	75/75	✓	72.49	63.2	10	61.67	13
		–	69.41				
	75/150	✓	69.14				
		–	63.03				
	75/300	✓	65.24				
		–	51.35				
	100/100	✓	55.78	47.4	11	49.39	7
		–	52.73				
	100/200	✓	53.8				
		–	48.91				
	100/300	✓	48.8				
		–	42.49				
	150/150	✓	39.25	31.6	14	32.93	9
		–	35.88				
	150/300	✓	38.09				
		–	33.77				

ledger beams on the interior face of the shear wall, *(ii)* sheathing boards having different sizes from the overall shear wall sizes and thus the presence of both vertical and horizontal seams, *(iii)* use of CP boards at the bottom stripe of the shear wall and *(iv)* different screw spacing in the top and bottom stripes from the middle part of the shear wall.

The key conclusions drawn from this study are as follows:

i. The floor and ceiling ledger beams create a portal action in the CFS frame which contributes by up to, respectively, 42 % and 27 % to the stiffness and peak lateral resistance of the shear wall.
ii. The sheathing's layout throughout the height of the shear wall should be consistent in terms of width in order to allow a proper rotation of the boards, and thus a full development of the sheathing-to-CFS screws shear capacity
iii. CP boards are required in the UK to be located at the bottom of external ground floor walls to avoid building up humidity. However, this study demonstrates that they negatively impact the lateral structural capacity of CFS walls, and can induce soft-story effects, in the case of walls with CP boards of 600 mm height. Therefore, their height should be minimized as possible.
iv. Sheathing-to-CFS screws located in the top and bottom stripes of the shear wall have less contribution to its lateral resistance, thus reducing the number of screws in these parts of the shear wall would not jeopardize its lateral capacity and results in a more economical structural design.
v. Finally, the comparison between the computational and code-based peak lateral resistance of the shear walls demonstrated that design codes should endeavor to include the effect of the constructional details studied in this paper.

In the future, further investigation will cover the effect of modular construction details on lateral behaviour of similar CFS shear walls with openings (*i.e.*, doors and/or windows).

CRediT authorship contribution statement

Smail Kechidi: Conceptualization, Methodology, Software, Validation, Formal analysis, Investigation, Visualization, Data curation, Project administration, Resources, Writing - original draft. **Ornella Iuorio:** Funding acquisition, Supervision, Conceptualization, Project administration, Writing - review & editing.

Declaration of Competing Interest

The authors declare that they have no known competing financial interests or personal relationships that could have appeared to influence the work reported in this paper.

References

[1] Iuorio O, Napolano L, Fiorino L, Landolfo R. The environmental impacts of an innovative modular lightweight steel system: The Elissa case. J Cleaner Prod 2019; 238:117905. https://doi.org/10.1016/j.jclepro.2019.117905.
[2] Raffaele L, Pali T, Bucciero B, Terracciano MT, Shakeel S, Macillo V, et al. Seismic response assessment of architectural non-structural LWS drywall components through experimental tests. J Constr Steel Res 2019;162:105575. https://doi.org/10.1016/j.jcsr.2019.04.011.
[3] Kechidi S, Bourahla N, Castro JM. Seismic design procedure for cold-formed steel sheathed shear wall frames: Proposal and evaluation. J Constr Steel Res 2017;128:219–32.

[4] American Iron and Steel Institute (AISI), North American standard for seismic design of cold-formed steel structural systems, AISI S400, Washington, D.C., USA, (2015).

[5] AS/NZS 4600: 2018. Cold-formed steel structures. Australian/New Zealand Standard, Sydney, Australia, (2018).

[6] Kechidi S. and Bourahla N., "Deteriorating hysteresis model for cold-formed steel shear wall panel based on physical and mechanical characteristics", *OpenSeesDays Portugal, Workshop on Multi-Hazard Analysis of Structures using OpenSees*, July 3-4, 2014, Porto, Portugal.

[7] Iuorio O, Fiorino L, Landolfo R. Testing CFS structures: The new school BFS in Naples. Thin-Walled Structures 2014;84:275–88.

[8] Iuorio O. Cold-formed steel housing. Pollack Periodica 2007;2(3):97–108.

[9] Fülöp LA, Dubina D. Performance of wall-stud cold-formed shear panels under monotonic and cyclic loading part I: experimental research. Thin-Walled Structures 2004;42(2):321–38.

[10] Branston AE, Chen CY, Boudreault FA, Rogers CA. Testing of light-gauge steel-frame - wood structural panel shear walls. Can J Civ Eng 2006;33(5):561–72.

[11] Liu O, Peterman KD, Yu C, Schafer BW. Impact of construction details on OSB-sheathed cold-formed steel framed shear walls. J Constr Steel Res 2014;101: 114–23.

[12] Stewart WG. The seismic design of plywood sheathed shear walls. New Zealand: University of Canterbury; 1987. Ph.D. thesis.

[13] Balh N. Development of seismic design provisions for steel-sheathed shear walls. Montreal, Québec, Canada: McGill University; 2010. Master thesis.

[14] Martínez-Martínez J, Xu L. Simplified nonlinear finite element analysis of buildings with CFS shear wall panels. J Constr Steel Res 2011;67(4):565–75.

[15] Liu P., Peterman K.D., Yu C. and Schafer B.W., "Characterization of cold-formed steel shear wall behavior under cyclic loading for CFS-NEES building", *Proceedings of the 21st International Specialty Conference on Cold-Formed Steel Structures*, October 24-25, 2012, St. Louis, Missouri, United States.

[16] https://opensees.berkeley.edu/wiki/index.php/Pinching4_Material.

[17] Lowes LN, Altoontash A. Modeling reinforced-concrete beam-column joints subjected to cyclic loading. J Struct Eng 2003;129(12):1686–97.

[18] Leng J, Peterman KD, Bian G, Buonopane SG, Schafer BW. Modeling seismic response of a full scale cold-formed steel-framed building. Eng Struct 2017;153: 146–65.

[19] Shamim I, Rogers CA. Steel sheathed/CFS framed shear walls under dynamic loading: Numerical modelling and calibration. Thin-Walled Structures 2013;71: 57–71.

[20] Vigh LG, Liel AB, Deierlein GG, Miranda E, Tipping S. Component model calibration for cyclic behavior of a corrugated shear wall. Thin-Walled Structures 2014;75:53–62.

[21] Ibarra LF, Medina RA, Krawinkler H. Hysteretic Models That Incorporate Strength and Stiffness Deterioration. Earthquake Eng Struct Dyn 2005;34(12):1489–511.

[22] Buonopane SG, Bian G, Tun TH, Schafer BW. Computationally efficient fastener-based models of cold-formed steel shear walls with wood sheathing. J Constr Steel Res 2015;110:137–48.

[23] Kechidi S, Bourahla N. Deteriorating hysteresis model for cold-formed steel shear wall panel based on its physical and mechanical characteristics. Thin-Walled Structures 2016;98:421–30.

[24] Padilla-Llano DA. A framework for cyclic simulation of thin-walled cold-formed steel members in structural systems. Blacksburg, United States: Virginia Polytechnic Institute and State University; 2015. Ph.D. thesis.

[25] Ngo H.H., "Numerical and experimental studies of wood sheathed cold-formed steel framed shear walls", MSc. Thesis, Johns Hopkins University, Baltimore, MD, United States, (2014).

[26] Derveni F, Gerasimidis S, Schafer BW, Peterman KD. High fidelity finite element modeling of wood-sheathed cold-formed steel shear walls. J Struct Eng 2021;147: 04020316.

[27] Derveni F, Gerasimidis S, Peterman KD. Behavior of cold-formed steel shear walls sheathed with high-capacity sheathing. Eng Struct 2020;225:111280. https://doi.org/10.1016/j.engstruct.2020.111280.

[28] Foliente GC. Stochastic dynamic response of wood structural systems. Virginia: Virginia Polytechnic Institute and State University Blacksburg; 1993. Ph.D. thesis.

[29] Nithyadharan M, Kalyanaraman V. Modelling Hysteretic Behaviour of Cold-Formed Steel Wall Panels. Eng Struct 2013;46:643–52.

[30] Nithyadharan M, Kalyanaraman V. A new screw connection model and FEA of CFS shear wall panels. J Constr Steel Res 2021;176:106430. https://doi.org/10.1016/j.jcsr.2020.106430.

[31] Iuorio O, Kechidi S, Banks N. Experimental investigation into the performance of cold-formed steel walls sheathed with OSB and cement-based panels. ce papers 2021;4(2-4):525–9.

[32] Peterman KD, Nakata D, Schafer BW. Hysteretic characterization of cold-formed steel stud-to-sheathing connections. J Constr Steel Res 2013;101(2014):254–64.

[33] BS EN 594 (1996). "Timber structures - Test methods - Racking strength and stiffness of timber frame wall panels," London, BSI.

[34] Fiorino L, Iuorio O, Landolfo R. "Experimental response of connections between cold-formed steel profile and cement-based panel", *The 19th International Specialty Conference on Recent Research and Developments in Cold-Formed Steel Design and Construction*, October 14-15, 2008, St. Louis, Missouri, United States.

[35] ECCS TC 7 TWG 7.10. "The testing of Connections with Mechanical Fasteners in Steel Sheeting and Sections", Number 124. ECCS/CIB. ISBN 92-9147-000-91. 2009. 2nd Edition.

[36] ECCS TC 7 TWG 7.9. "Preliminary European Recommendations for the Testing and Design of Fastenings for Sandwich Panels", Number 127. ECCS/CIB. ISBN 92-9147-000-93. 2009.

[37] BS EN ISO 6892-1 (2016). "Metallic materials. Tensile testing. Method of test at room temperature," London, BSI.

[38] EN 1993-1-3, Eurocode 3 (2007). "Design of steel structures, Part 1.3: general rules for cold formed thin gauge members and sheeting," European Committee for Standardization, Brussels, CEN.

[39] ABAQUS (2017). "Abaqus theory guide." *Version 2017*, Dassault Systems Simulia Corp., United States.

[40] Schafer BW, Li Z, Moen CD. Computational modeling of cold-formed steel. Thin-Walled Structures 2010;48(10-11):752–62.

[41] Kechidi S, Fratamico DC, Schafer BW, Castro JM, Bourahla N. Simulation of screw connected built-up cold-formed steel lipped channels under axial compression. Eng Struct 2020;206:110109.

[42] Koubek R, Dedicova C. Friction of wood on steel. Sweden: Linnaeus University; 2014. Master thesis.

[43] Ding C. "Monotonic and cyclic simulation of screw-fastened connections for cold-formed steel framing", MSc. thesis. Virginia Tech, Blacksburg, VA: United States; 2015.

[44] MATLAB 2019b, The MathWorks, Inc., Natick, MA., United States, 2020.

[45] SCI ED002 (2003). "Lightweight steel/timber composite solutions: information and guidance for new product development", Steel Construction Institute, United Kingdom.